Geophys. J. Int. (1994) **116,** 754–783

A geodynamic framework for interpreting crustal-scale seismic-reflectivity patterns in compressional orogens

Christopher Beaumont[1] and Garry Quinlan[2]

[1]*Oceanography Department, Dalhousie University, Halifax, Nova Scotia,* B3H 4J1, *Canada*
[2]*Earth Sciences Department, Memorial University, St John's, Newfoundland,* A1B 3X5, *Canada*

Accepted 1993 August 16. Received 1993 August 6; in original form 1993 January 21

SUMMARY

2-D, plane-strain finite-element models are used to calculate crustal deformation patterns within model compressional orogens and the results are compared with natural examples. The fundamental driving mechanism for model deformation is provided by asymmetric detachment and underthrusting of mantle lithosphere, with deformation being rooted at the stress singularity where the mantle detaches. Deformation steps up into the overlying crust and spreads laterally according to the rheological properties assumed for the crust. The crust is modelled using plastic (frictional) and viscous rheologies and incorporates the effects of compositional layering and variable geothermal gradients. Overall deformation is determined by balancing the internal strength of the crust against the sum of applied boundary stresses plus the gravitational stress induced by mass redistribution within the deforming orogen. The amount of convergence in the models is limited to 150 km or less and so the results are not strictly comparable with larger orogens involving greater convergence. Nevertheless, larger orogens seem to evolve through stages that may be understood in terms of the models provided that consideration is confined to smaller scale components that are limited in time and space. The continuum deformation calculated by the finite-element models is qualitatively converted to equivalent patterns of discrete faults and shear zones by associating these discrete features with the areas of highest cumulative strain using the results of sandbox experiments as guides. Significant styles of deformation include: (1) coupling between step-up shears and subhorizontal detachments at one or more levels; (2) localization of upper crustal deformation by subduction of the lower crust; and (3) pinning of deformation by surface denudation.

A partial catalogue of such model styles is presented in which the strength of basal coupling between crust and mantle, the number of rheological layers within the crust, the thickness of subducted lower crust, and the extent of surface denudation are varied systematically. Compressional orogens with a wide range of ages are characterized by crustal-scale seismic reflectivity similar to patterns of fault/shear zones represented in this catalogue of styles. This similarity suggests that crustal-scale seismic-reflection data can be used to constrain the dynamic processes involved in compressional orogenesis.

Key words: compressional orogens, crustal seismic reflectivity, finite elements, geodynamics, subduction.

INTRODUCTION

Crustal-scale seismic-reflection surveys have been undertaken in a wide variety of tectonic regimes of ages ranging from Precambrian (Green *et al.* 1988) to modern (Stern & Davey 1989). The available data have been used to address general topics such as the nature of the crust–mantle boundary (Mooney & Brocher 1987; Hall 1989) and the physical properties and composition of the lower crust (Hurich & Smithson 1987; Wenzel, Sandemeier & Walde

1987). However, most deep-seismic-reflection profiles have been used as a basis for models addressing the tectonic evolution of those regions from which the data were collected (Meissner *et al.* 1991; and references cited therein).

The physical origin of reflectivity in crystalline rocks is a matter of some debate, being largely attributed to mylonitic shear zones, fluid-filled faults and lithological boundaries (Klemperer *et al.* 1987). The first two of these are manifestations of strain concentrations associated with ductile and brittle deformation, respectively. Lithological contrasts may, but need not necessarily, result from juxtaposition across faults or within shear zones and so these may also be a consequence of localized strain.

The use of crustal-scale seismic-reflection data in tectonic analyses implicitly assumes a connection between patterns of reflectivity and tectonic processes. Two end-member situations can be envisaged. At one end of the spectrum, all reflectors are inherited from earlier tectonic episodes and only translated or rotated during orogenic deformation. At the other end, all reflectors are created by strain associated with orogenic deformation through mechanisms such as those mentioned above. Any orogenic belt is likely to contain examples of each of these end-members as well as intermediate cases of inherited reflectors disrupted and rearranged by orogenic deformation.

One way to evaluate where actual compressional orogens fall within this continuum of inherited versus newly generated reflectivity is to examine seismic profiles from several different compressional orogens. Similarity among the observed patterns argues for the importance of newly generated reflectivity because translation and rotation of reflectors inherited from diverse tectonic histories are unlikely to produce a common pattern. Quinlan, Beaumont & Hall (1993) have demonstrated that many compressional orogens do contain a recurring pattern of reflectivity. For this reason we believe that a significant proportion of the seismic reflectivity observed in such orogens results from the tectonic processes by which the orogens are constructed. At least two of the physical processes suggested to produce reflectivity (Klemperer *et al.* 1987) are manifestations of strain and so we believe that seismic reflectivity records, for the most part, patterns of strain developed as a consequence of crustal compression. If this association of seismic reflectivity with strain is correct, what does it reveal about the processes involved in building compressional orogens?

The development of a seismically based tectonic model generally proceeds in three stages. First, a crustal scale reflection profile is examined and the major reflectors are highlighted. Second, these reflectors are assigned geological significance based on their orientation and spatial relationship with known features of surface geology. Finally, a tectonic interpretation is based on the geometric relationships between reflectivity patterns combined with what is known independently from regional geological relationships and other geophysical data. Models constructed in this manner are inevitably kinematic and do not address the dynamic processes involved in crustal deformation. For this reason it is difficult to know whether a proposed model is dynamically feasible or under what circumstances it may be applicable elsewhere.

This paper uses finite-element models to examine the dynamics of compressional orogens and to test the hypothesis that crustal deformation in small orogens (those with less than about 200 km of convergence following ocean closure) is governed by the motion of the underlying lithosphere. Deformation is assumed to be the crustal expression of detachment and underthrusting of the mantle lithosphere at the location where two plates converge. Our belief that reflectivity patterns in compressional orogens are largely a consequence of tectonics leads us to use our models first to focus on the strain estimates associated with this mechanism of crustal deformation and then to compare them with observed reflectivity patterns. We will return later to a discussion of the preservation and superposition of reflectivity produced by earlier tectonic episodes.

A range of synthetic strain patterns is associated with different combinations of model boundary conditions and crustal rheology. These patterns are shown to have many similarities with seismic reflectivity patterns observed in compressional orogens. If, as argued here, these patterns record strain, then this similarity suggests that the crust has preferred modes of deformation that are rheologically controlled and can be excited by boundary stress conditions. An understanding of how the synthetic strain patterns evolve provides a process-oriented framework within which to interpret the tectonic significance of crustal-scale seismic-reflectivity patterns.

MODELLING APPROACH AND ASSUMPTIONS

Figure 1 illustrates the basic elements of our geodynamic models. 2-D plane-strain finite-element models are deformed by the application of a basal velocity boundary condition. This kinematic basal boundary condition, which solutions are required to obey, assumes that the mantle lithosphere detaches from the crust and underthrusts adjacent mantle lithosphere at the point labelled S in Fig. 1. The velocity relative to S is non-zero on the underthrusting side (referred to as the 'pro' side) and zero on the overthrusting side (referred to as the 'retro' side). This corresponds to a situation in which the underthrusting mantle behaves in an essentially rigid manner and is one end-member of the possible ways in which the mantle lithosphere may respond to compression. We make no attempt to evaluate the dynamic requirements for such detachment and underthrusting to occur. Instead, we address its consequences by predicting the style of crustal deformation and strain partitioning forced by such a process. Although this basal boundary condition is kinematic, estimates of velocity, strain rate, stress, deformation and cumulative strain fields of the models, together with the geometry of the free surface and the flexurally supported base, are determined by internally consistent dynamic calculations (Fullsack 1994).

Figure 1 shows that the initial response of the system is to focus strain and deformation above the basal velocity discontinuity at point S. The crust is compressed and thickened while the mantle lithosphere is removed by subduction. Our models assume the crust to have laterally uniform mechanical properties. By ignoring lateral strength differences in the crust we assume that any embedded geometrical, compositional or structural properties of the

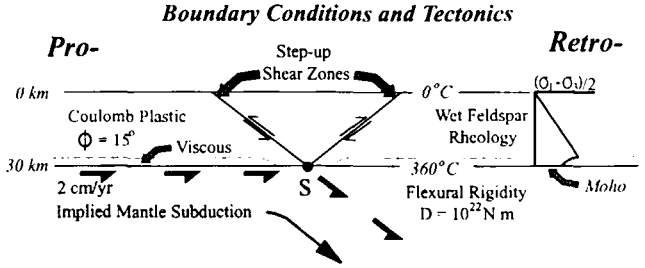

Figure 1. Elements of the basic plane-strain model of crustal deformation under basal velocity boundary conditions that correspond to the convergence between two rigid lithospheric mantles, one of which (shaded) detaches at point S and is subducted beneath the other. The model includes only the laterally uniform crustal layer, the basal boundary conditions, and an underlying floating elastic beam that provides flexural isostatic support. Velocities are specified with respect to S. To the left of S in the 'pro' region the horizontal basal velocity is uniform (2 cm yr $^{-1}$). To the right of S in the 'retro' region the basal velocity is zero. the crustal layer has an incompressible non-cohesive Coulomb plastic rheology with an angle of friction $\phi = 15°$, which gives an increasing yield strength with depth as shown diagrammatically at the right. The strength envelope is limited by the brittle–ductile transition for wet feldspar deformation. The depth of this transition to power-law viscous creep depends on the ambient strain rate (or, equivalently, stress) and the temperature, and is determined dynamically as part of the finite-element model solution. In Model 1 the basal temperature is 360 °C, which limits power-law viscous creep to a thin basal layer. In other models the temperature gradient, crustal composition and basal boundary conditions are modified (see Fig. 4). Deformation of the model is calculated using a velocity-based Eulerian finite-element model in which the grid is modified as the crustal layer thickens.

crust are less important in determining deformation than are the boundary conditions driving deformation. The similarity between our model results and observed seismic patterns, established later in this paper, provides a basic justification for this assumption, but the role of mechanical inhomogeneities in orogenic evolution will be addressed explicitly in future work.

The properties of these geodynamic models are similar, but not identical, to the basic model discussed by Willett, Beaumont & Fullsack (1993). The base in the present models is flexurally supported by a continuous elastic beam with flexural rigidity of 10^{22} N m, whereas the Willett *et al.* (1993) basic model has a rigid base. Flexural support allows for the consideration of isostatic effects in evolving orogens. In the two approaches the crustal layer is a rigid, perfectly plastic, incompressible material with a non-cohesive Coulomb yield criterion having a coefficient of internal friction ϕ. In the Willett *et al.* (1993) model the base of the crustal layer also has a Coulomb yield criterion but with a different coefficient of friction, ϕ_b, meant to simulate a low-strength layer at the base of the crust. In the models discussed here the deformation mechanism throughout the crustal layer is either frictional Coulomb plasticity, with a common coefficient of friction ϕ, or thermally activated power-law creep, depending on which mechanism produces the greater strain rate under ambient conditions. The transition between these two alternative mechanisms depends on temperature, the mineralogical composition of the model crust and the assumed convergence velocity.

The appropriate values of parameters describing power-law creep depend on the petrological composition of the crust. The various models discussed in this paper assume that the crust can be approximately represented by different combinations of 'wet' quartz and 'wet' feldspar. Accordingly, the creep parameters are based on laboratory deformation mechanisms for these minerals (Shelton & Tullis 1981; Jaoul, Tullis & Kronenberg 1984; Ord & Hobbs 1989).

There is considerable uncertainty as to whether ductile deformation in the crust is appropriately represented by power-law creep with these parameter values. The deformation styles of the models are, however, relatively insensitive to the details of the viscous rheology. We characterize these models in terms of temperature. We refer to them as cold, warm, or hot to imply that the effective viscosity at the base of the crustal layer is high, intermediate, or low and that the shear strength of the viscously deforming regions is correspondingly similar to, lower than, and very much lower than the Coulomb yield strength at comparable depths.

The same range of shear strength can be achieved by many different parameter combinations. Consequently, no importance should be attached to the choice of temperature and mineralogy used in the models. We do not believe that the Earth's crust is this simple. However, it may have intrinsically weak and strong layers of frictional and viscous materials and it is the behaviour of this type of laminate that we wish to investigate.

The finite-element techniques used in deriving the model solutions are not discussed here but are described in detail, together with an analysis of their accuracy, by Fullsack (1994). Instead, we focus on the model geometry and the predicted pattern of shear zones and seek to relate these to seismic-reflectivity patterns.

MODEL 1. BASIC MODEL: COLD, ONE-LAYER CRUST, MANTLE SUBDUCTED

The geometry, boundary conditions and crustal properties of Model 1 are those described in the preceding section and illustrated in Fig. 1; i.e. it is assumed that mantle lithosphere subducts beneath the laterally adjacent crust–mantle boundary. The rheological behaviour of the model crust is that of 'wet' feldspar. The geothermal gradient is linear (12 °C/km) between a surface temperature of 0 °C and a Moho temperature of 360 °C at a depth of 30 km. The basal velocity of the underthrusting plane is 2 cm yr $^{-1}$ relative to the mantle detachment point, S.

Model 1 results

In Model 1 the feldspar rheology and low basal temperature combine to produce Coulomb frictional deformation throughout the crust in the region of the detachment point, S, where the boundary conditions require strain rates and stresses to be high. Elsewhere, where strain rates are lower, the crustal layer is coupled to the kinematic boundary conditions by a strong viscous base (Fig. 1).

Initial failure occurs on two conjugate shear zones (Fig. 2a) that root at the stress singularity, S. Consistent with the earlier defined terminology, we refer to these shears as the

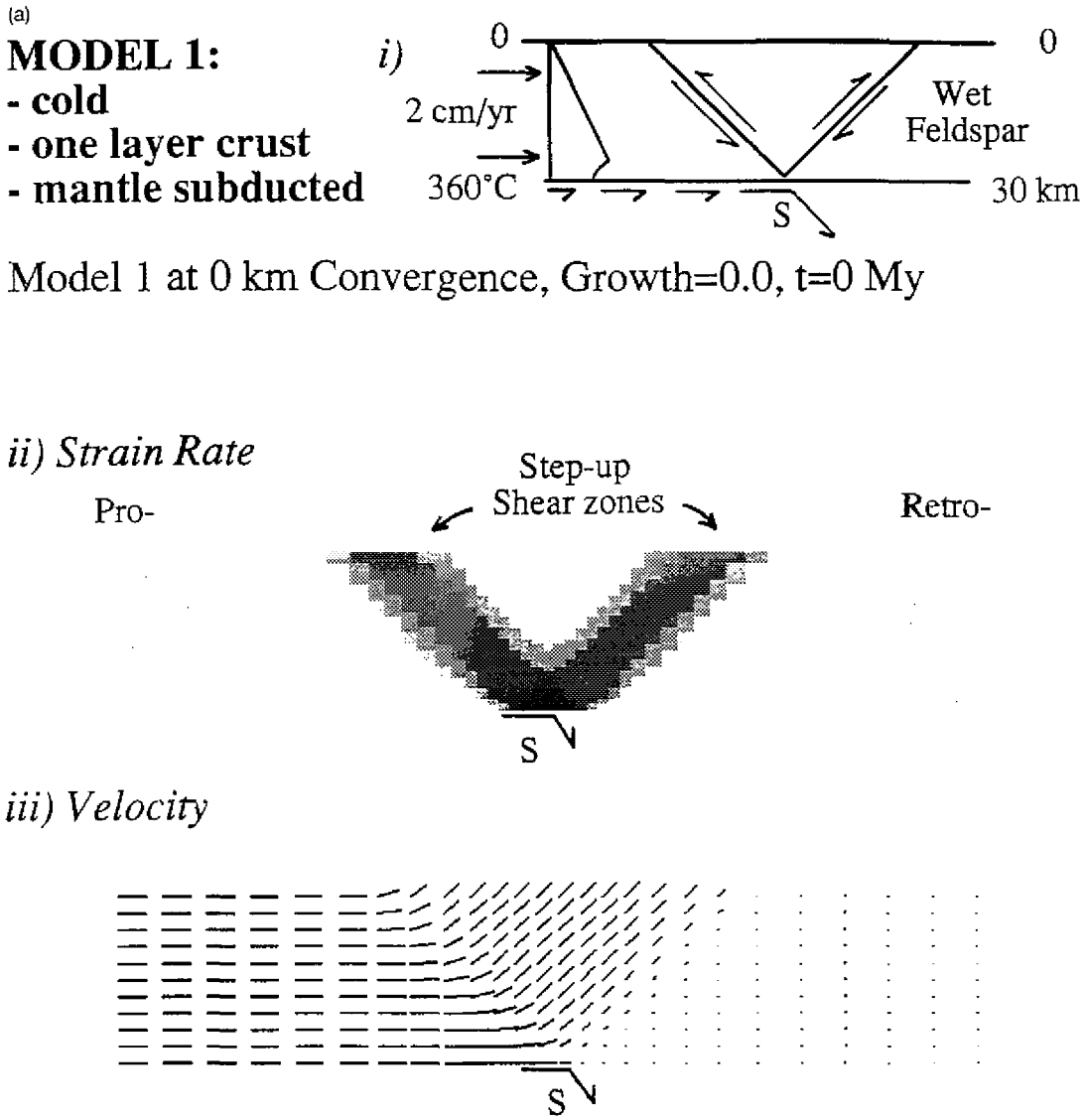

Figure 2. Model 1 Results. (a) Convergence 0 km. (a, i) Model properties and deformation style. Growth = convergence/initial layer thickness. (a, ii) Finite-element model strain rate. Darker shades of grey correspond to increasing strain rates $\dot{\varepsilon}$; $\dot{\varepsilon} < 10^{-15}\,s^{-1}$ (pale grey), $10^{-15}\,s^{-1} < \dot{\varepsilon} < 10^{-14}\,s^{-1}$ (medium greys), $\dot{\varepsilon} > 10^{-14}\,s^{-1}$ (darkest greys). These scales are used for all subsequent models. (a, iii) Velocity field with sense of convergence from left to right. Length of line is proportional to magnitude of velocity. (b) Convergence 40 km. (b, i) Velocity and strain rate. (b, ii) Deformation, shown by a Lagrangian mesh used to track total displacements, and by deformation of passive grey marker layers that were initially horizontal and uniformly thick. Note asymmetry of deformation and tectonic elements. The position of the basal detachment is shown by the arrow. (b, iii) Magnitude of total logarithmic strain. Progressively darker shades of grey correspond to increasing strain, ε. $\varepsilon < 0.1$ (palest grey), $0.1 < \varepsilon < 1.0$ (medium greys), $\dot{\varepsilon} > 1.0$ (darkest greys). These scales are used for all subsequent models. The lines illustrate the style of seismic reflectivity fabric that we anticipate if the strain were distributed on discrete thrust planes as seen in sandbox models (Fig. 3). The lines are highly stylized with widths and continuity that increases with the total strain. (c) Convergence 100 km. (c, i) Velocity and strain rate. Note the decrease in dip of the step-up shears and limited detachment of the crust from its base. (c, ii) Deformation. Note crustal thickening, distributed deformation in the pro-wedge and focused deformation in the retro-wedge that creates a crustal-scale shear zone. (c, iii) Magnitude of logarithmic strain with overlay of stylized reflectivity fabric. Note apparent truncation of pro-wedge reflectors by reflectors in the retro-shear which is caused by transport of deformed pro-wedge material up the hanging wall of the retro-shear zone.

pro- and retro-step-up shears. Although the velocity is asymmetric with respect to point S (Fig. 2a, iii), the strain rate within each of the shears is the same and they bound a rigid triangular block that is translated retro-ward up the handing wall, or retro-shear zone.

With continued convergence the model goes through three development stages. Stage 1 involves block uplift (Fig. 2a). Stage 2 involves the development of a pair of outwardly dipping crustal-scale tectonic wedges, a low taper-angle pro-wedge and high taper-angle retro-wedge (Fig. 2b). Stage 3 involves the development of a low taper segment of the retro-wedge (Fig. 2c). These different stages are discussed in detail by Willett *et al.* (1993) and Beaumont, Fullsack & Hamilton (1994).

Figure 2(b, i) shows the velocity and strain-rate distribution after 40 km of convergence. The amount of

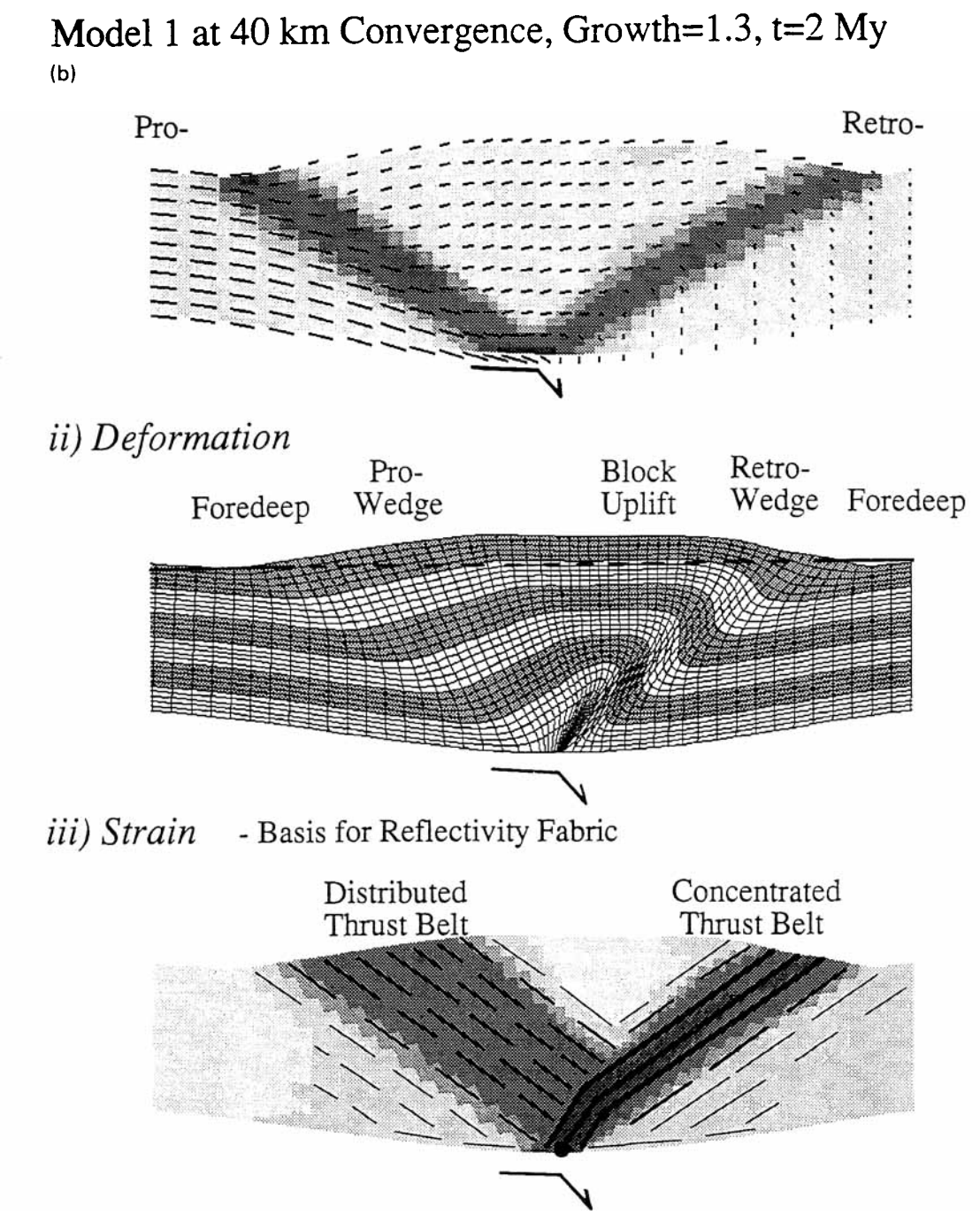

Figure 2. (*Continued.*)

mass that has entered the model orogen at this stage depends not only on the amount of convergence, but also on the original thickness of the model layer (the only length-scale in the model). To characterize model results in a way that is largely independent of layer thickness, we define the 'normalized convergence', or 'growth' as the ratio of the amount of convergence to the initial thickness of the model layer. If mass does not leave the model orogen, as, for example, by erosion or lower crustal subduction, this measure reflects the increase in mass, or the growth, of the orogen. As the initial thickness of the model layer in Fig. 2 is 30 km, 40 km of convergence corresponds to a 1.3 growth factor.

Note that the shear zones in Fig. 2(b, i) have rotated to a lower dip than in Fig. 2(a) but still root at the mantle detachment point S. The region between the shears is occupied by an uplifted block, the pro-wedge and the retro-wedge. If the basal layer is frictional, these wedges would be the minimum and maximum taper compressive Coulomb wedges described by Dahlen (1984). In this

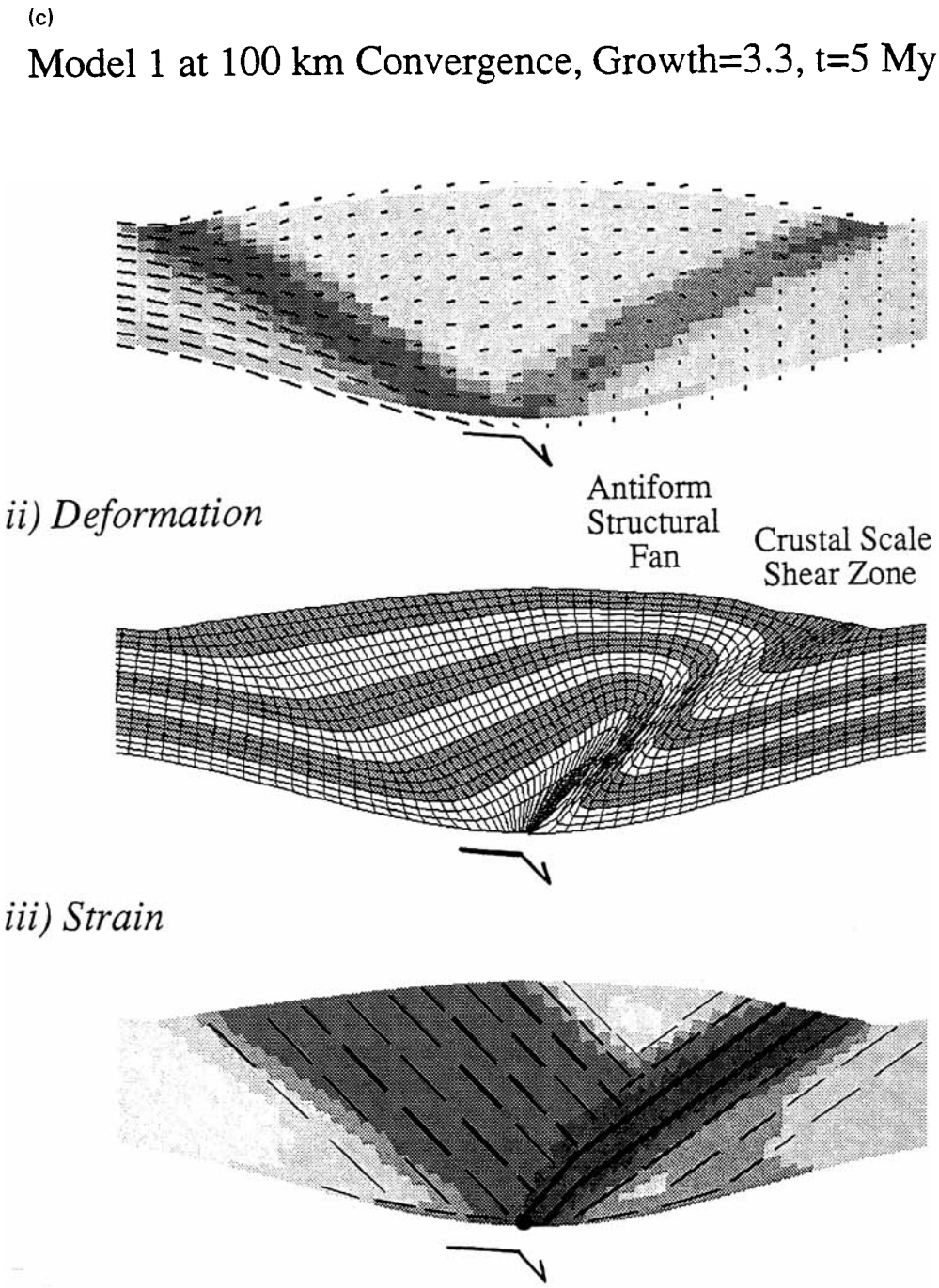

Figure 2. (*Continued.*)

instance the wedges grow on a base that is partially frictional and partially viscous, therefore the basal strength and taper depend on the strain rate and effective viscosity. The main characteristics are, however, very similar to critical Coulomb wedges.

Although both step-up shears have the same strain-rate distributions, their effect on the model material is very different because convergence is asymmetrical. During stage 1 (Figs 2a, ii and a, iii), for example, material is carried through the pro-step-up shear from left to right. The strain or deformation imparted to this material is the product of the strain rate in the shear zone and the time the material takes to cross the shear zone. The overall effect is to produce a zone of moderate strain distributed through all the material that has crossed the pro-shear zone and entered the pro-wedge (Fig. 2b, iii). In contrast, the horizontal component of material velocity is much smaller in the retro-shear (Fig. 2b, i), with the result that material remains trapped within the retro-shear developing a narrow zone of highly sheared material (Fig. 2b, ii and b, iii). It is this basic difference between the step-up shears, imparted by asymmetrical convergence, that is responsible for the

distributed deformation of the pro-wedge and the localized deformation of the retro-wedge during development stages 1 and 2. The retro-wedge corresponds to what geologists normally call a shear zone—a package of rocks in which the relative positions of the rocks and zone of high shear strain rate remain the same. The pro-step-up is different because the rocks move with respect to the zone of high shear strain rate.

Cumulative deformation (Fig. 2b, ii) is indicated by the current position of shaded marker layers that were originally horizontal. This figure shows the elements of the deformed layer in a way that emphasizes the asymmetry of the compressional system and the structural antiform that grows as material is obducted up the hanging wall of the retro-step-up shear. The two foredeeps are created by flexural isostatic compensation of the weight of the thickening layer and would not be present if the model base was rigid.

The corresponding magnitude of cumulative strain (Fig. 2b, iii) shows two dipping zones of high strain bounding the block uplift. We interpret these zones to be equivalent to two conjugate belts of folding and thrusting, which at a crustal scale would be a large-scale structural fan (Brown, Beaumont & Willett 1993).

Figure (2c) shows Model 1 at 100 km convergence, growth = 3.3. The layer has doubled its thickness and is beginning to detach pro-ward along its base as it enters development stage 3. The pro-wedge is about 100 km wide and the antiform has grown so that the structural relief across the retro-step-up shear is 25 km. The whole process only takes 5 Myr at the modest 2 cm yr^{-1} convergence rate.

Comparison with sandbox models

The results of a sandbox experiment that has the same boundary conditions as Model 1 (Malavieille 1984), except that the base is rigid, shows the same deformation style (Fig. 3), i.e. pro-wedge, block uplift and retro-wedge. Other small differences are that dry sand has a higher internal angle of friction, about 30°, than Model 1, $\phi = 15°$, and the base of the sand layer is also frictional. These differences make the surface slopes of the sand model steeper than those of Model 1, but the geometrical relationships remain the same. The difference that is significant for this discussion is that the deformation in the sand has occurred on a series of discrete shears or fault-like structures. The finite-element model predicts the same total strain but distributes it continuously throughout the deformed region.

The Earth's crust certainly deforms by faulting and shearing on discrete planes, like sand, and these planes act individually or collectively as seismic reflectors. This statement is corroborated by specific examples in which the reflectivity fabric corresponds to the dip projection of fault and shear zones exposed at the surface (e.g. Hurich *et al.* 1985; Litak *et al.* 1991). By analogy with the sandbox experiments and the specific examples where the reflectivity fabric is known to be related to deformation, we interpret the regions of high strain to be regions of seismic reflectivity fabric. Fig. 2(c, iii) shows the type of fabric that we expect on the basis of the thrusting style of the sandbox. The pattern is merely a stylized prediction without any attempt to quantify the form of the reflectors. The part of this interpretation that should be valid is the geometrical relationships among packages of reflectors and we concentrate on this geometry and the inferred truncation relationships.

EFFECTS OF TEMPERATURE, DENUDATION AND SUBDUCTION

In a series of models, Models 2–9, we investigate how the basic style of deformation and predicted reflectivity fabric changes with the surface boundary conditions and internal properties of the deforming layer. The results are a partial catalogue of styles that we expect in models of small compressional orogens where deformation is controlled by subduction. Fig. 4 shows the relationships among the model

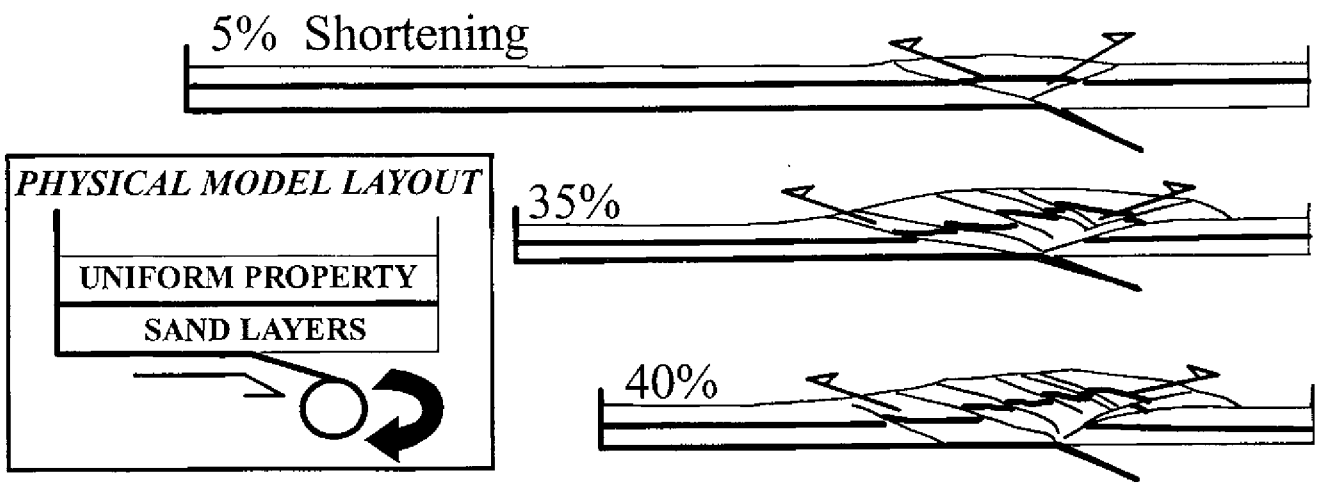

Figure 3. Results of a sandbox experiment with the same bondary conditions as Model 1 (Figs 1 and 2) (modified from Malavieille 1984). Horizontal layers are passive markers. Note discrete shears and fault-like structures that form at the step-up shear zones and the basal detachment that develops beneath the pro-wedge. We use these discrete structures to infer crustal-deformation style and seismic-reflectivity fabric.

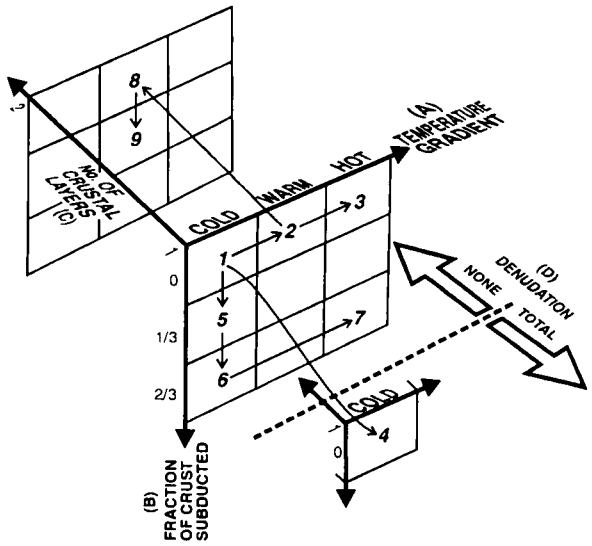

Figure 4. Block diagram showing relationships among the properties of Models 1–9 in terms of the principal controlling factors. (A) Temperature gradient in the crust (cold, warm, hot models); (B) fraction of the crust that is subducted (zero corresponds to mantle subduction and unity would be total crustal subduction; (C) number of compositional layers in the crust; (D) denudation, is shown separately. The arrows between models show their primary relationships. Model 4 is a special case which is equivalent to Model 1 except that it is totally denuded. Although only a subset of the 36 possible parameter combinations are presented in Models 1–9, the primary characteristics of other models can be inferred by interpolation.

properties as variations on Model 1. Models 2 and 3 investigate the effect of increasing geothermal gradient. Model 4 is a modification of Model 1 in which erosion of the upper surface prevents tectonic thickening of the model crustal layer. It is intended to illustrate the coupling between tectonics and surface processes. The effects of erosion will also modify the tectonic and reflectivity styles of all the other models. Models 5 and 6 investigate the consequences of increases in the amount of crustal, as well as mantle, subduction of the pro-ward lithosphere. Model 7 combines a high geothermal gradient with crustal subduction. Model 8 is the equivalent of Model 2 but has a two-layer crust. Model 9 adds crustal subduction to Model 7. The suite of models presented is incomplete (Fig. 4), but serves to illustrate how simple modifications to the basic model can produce important changes. The model results are illustrated in the same way as those for Model 1. To limit the number of figures, model results are shown at only one stage of convergence, usually 40 km. Similarly, we limit the discussion of the results to important points that are relevant to the tectonics and anticipated seismic-reflectivity character of the models.

Model 2: warm, one-layer crust, mantle subducted

An increase in the thermal gradient from 12 to 15 °C/km is sufficient to make the basal part of the model crustal layer entirely viscous and weaker than the maximum strength of the overlying Coulomb region (Fig. 5i). The model evolves through the same three stages as Model 1, but enters stages 2 and 3 with less convergence. Fig. 5 shows the model at 75 cm convergence. The pro-wedge, block uplift and retro-wedge tectonic components are evident, but deformation is distributed across a wider region than in Model 1 because the deforming layer has detached from its base in both the pro- and retro-directions. The pro- and retro-wedges contain one or more transient plug uplifts so that deformation is achieved by both forward-verging and backward-verging thrusts. This deformation style is also seen in sandbox experiments where the base is weak compared with the sand layer (Huiqi, McClay & Powell 1992, Fig. 6). Note that the increasing compression of Model 2 is accompanied by the development of successive second-order pairs of oppositely vergent step-up shear zones at greater distances from the mantle detachment point.

The strain distribution and inferred seismic-reflectivity fabric is similar to Model 1 except that it is distributed over a wider zone of less intense shear. Deformation that is focused on the basal shear zone or an equivalent detachment is also expected to contribute to the reflectivity fabric, perhaps in the form of a narrow band of subhorizontal reflectors that are strongest near the mantle-detachment singularity and decrease laterally towards the deformation fronts of the wedges.

Model 3: hot, one-layer crust, mantle subducted

A further increase in the thermal gradient to 20 °C/km creates a crustal layer in which the lower half is viscous. The basal region is weak relative to the maximum Coulomb strength of the upper half of the layer, and it therefore shears easily with respect to the base (Fig. 6). Again, the model evolves through stages 1–3 and has the same tectonic elements as Models 1 and 2. However, these elements are much more subdued. After only 40 km of convergence basal detachment has spread approximately 100 km pro-ward and retro-ward of the singularity. Much of the deformation of the layer occurs as pure shear thickening above a lower crustal simple shear zone. The antiform is weakly developed and there is little asymmetry between the two wedges. The strain is still marked by the two wedges bounding the uplifted plug but the predicted reflectivity fabric (Fig. 6iii) may be less intense than for Model 1 if the reflector intensity is related to the amount of strain. In Model 3 the subhorizontal component of reflectivity related to detachment shear strain in the lower crust is predicted to be more important than in Model 2.

Model 4: cold, one-layer crust, mantle subducted, surface denuded

In Model 4 we return to the basic cold crust of Model 1 but remove all crustal material that is tectonically uplifted above the initial surface. This is an extreme example of a rapidly denuded orogen and serves to demonstrate the feedback coupling between tectonics and surface processes. Because the convergent mass is removed by erosion there is no tectonic thickening or flexural isostatic subsidence of the model crustal layer (Fig. 7). As a consequence the velocity field and strain-rate distribution change very little throughout the evolution of the model and then only as a consequence of the advection of the materials and the

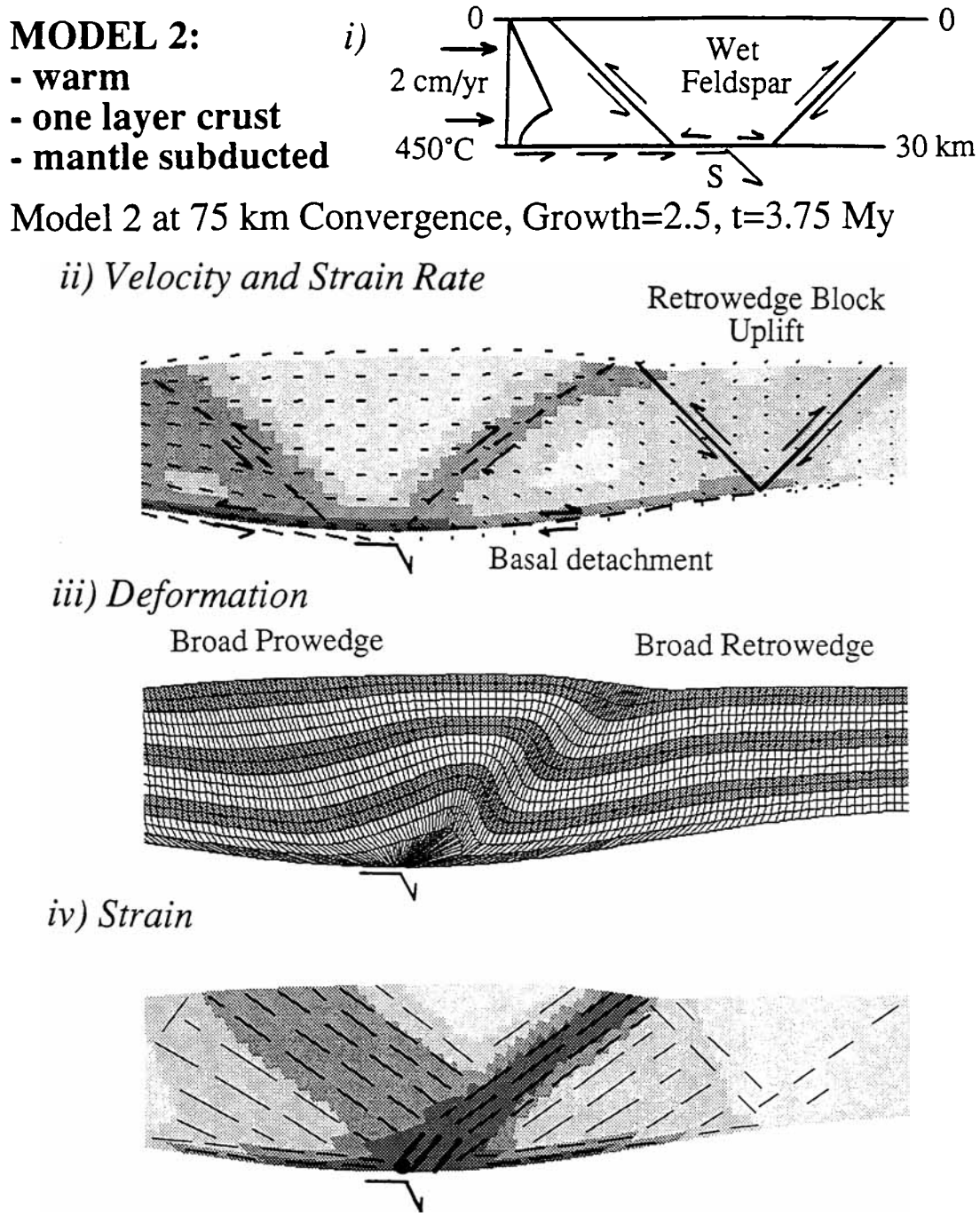

Figure 5. Model 2 results. (i) Model properties and style of deformation. (ii) Velocity and strain rate. Note basal shear zone and secondary block uplift which develops when growth >2. As convergence increases more of these block uplifts develop on both the pro-and retro-sides of the orogen. (ii) Deformation shown by Lagrangian mesh and grey marker layers. (iv) Magnitude of logarithmic strain with stylized seismic-reflectivity-fabric overlay (grey scales are same as those for Model 1).

temperature field. Even the viscous material that is uplifted in the antiform (Fig. 7iii) passes through the 'brittle–ductile' transition because the yield strength decreases as the pressure is reduced. It therefore behaves as a Coulomb material even though its temperature is higher than the surrounding material.

The result (Figs 7iii and iv) is a narrow, highly deformed orogen in which the lower crust has been exhumed to the surface after 2 Myr and only 40 km of convergence. It should be contrasted with Model 1 (Fig. 3b). The inferred seismic-reflectivity pattern for Model 4 is similar to that of Model 1 except that the step-up shears are steeper. The pro-wedge reflectivity has nearly been advected to the surface in the hanging wall of the retro-step-up shear because the block uplift has been eroded. Instead of the pro-ward advance of the pro-wedge seen in Model 1, the narrower pro-wedge is confined to the triangular region originally occupied by the block uplift.

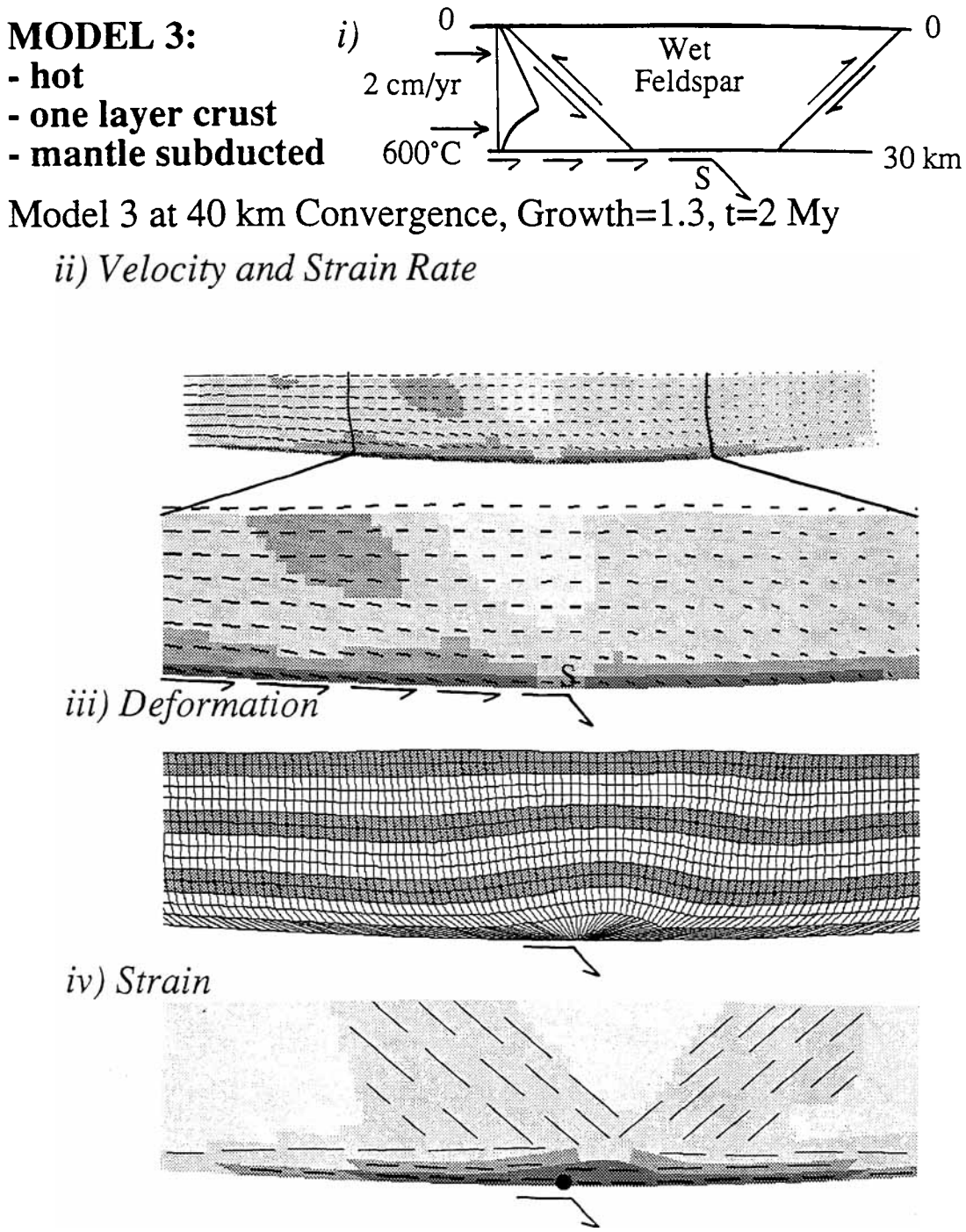

Figure 6. Model 3 results. (i) Model properties and style of deformation. (ii) Velocity and strain rate. Upper panel shows total model, whereas lower panel shows magnification of central region. (iii) Deformation shown by Lagrangian mesh and grey marker layers. Note weakly developed antiform, nearly pure shear deformation in most of the crustal layer and simple shear of basal shear zone. (iv) Magnitude of logarithmic strain with stylized-reflectivity fabric overlay. Note low strain distributed over a wide region and high strain in basal shear zone.

Model 5: cold, one-layer crust, one-third crust subducted

Model 5 has the basic cold crust of Model 1, but the basal boundary condition is changed to include a flux of material through the base of the model that is equal to one-third of the convergent crustal mass flux (Fig. 8i). To show the most simple deformation style associated with this lower crustal subduction, the existing material velocity vectors dip at 45°, parallel to the preferred failure planes of the step-up shears in an incompressible Coulomb material. These boundary conditions excite one internal mode of deformation: the cross mode. When the exiting flux has a lower dip angle, such as is the case with many oceanic subduction zones, more than one mode of deformation is excited. This leads to complexity that is beyond the scope of the work presented here. It is important to note that only the basal boundary

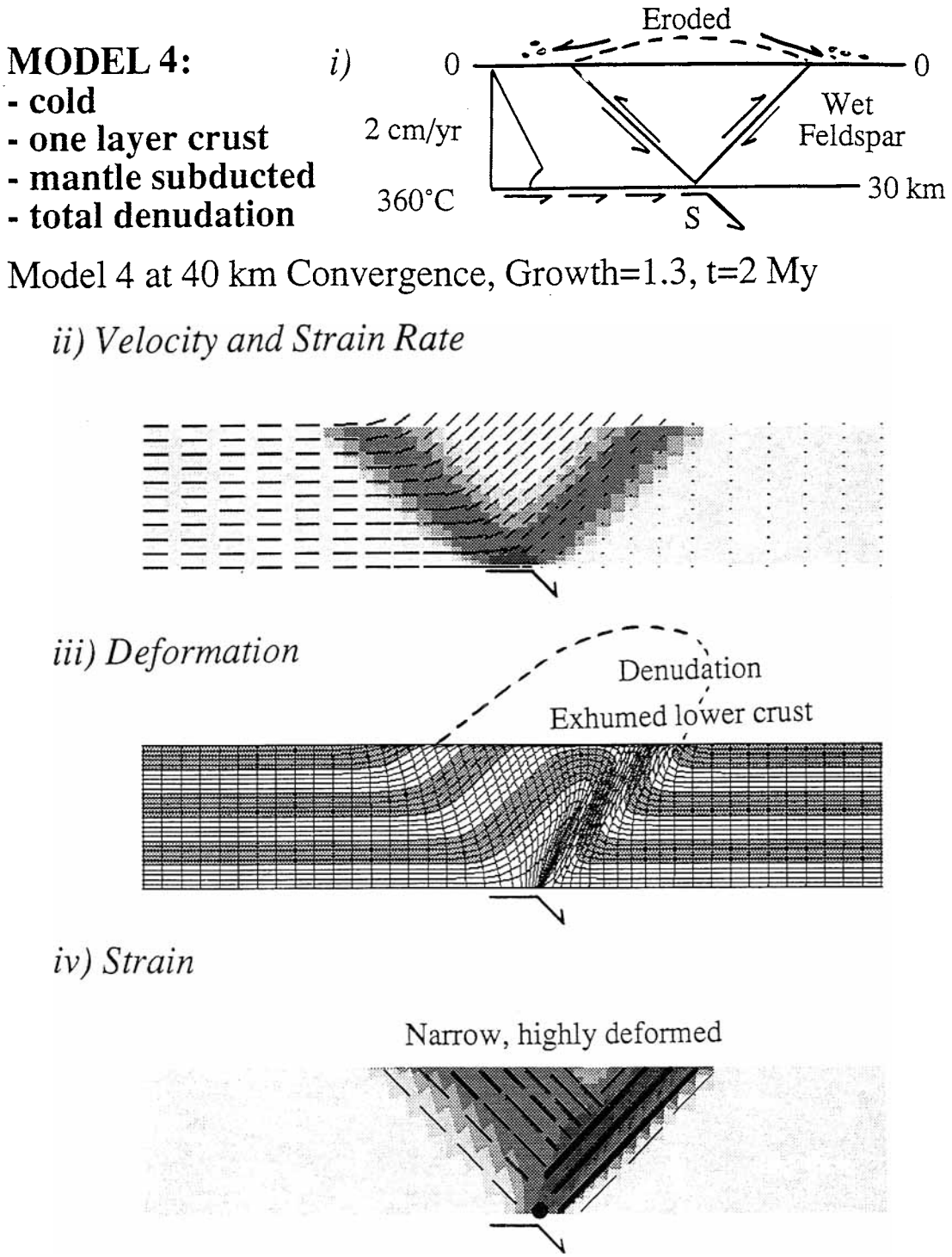

Figure 7. Model 4 results. (i) Model properties and style of deformation. Note total erosion of uplifted surface material. (ii) Velocity and strain rate. These remain constant in this model because the geometry does not change. (iii) Deformation shown by Lagrangian mesh and grey marker layers. Note strongly developed antiform, cumulative denudation and exhumation of the lower crust. (iv) Magnitude of logarithmic strain with stylized-reflectivity fabric overlay. Note narrow region of deformation.

condition, corresponding to mantle subduction with a strongly attached piece of lower crust, is specified. The internal strain partitioning, velocity field and deformation are determined by a dynamic solution of the layer deformation under these boundary conditions.

Initial failure occurs on two planes that are equivalent to the pro- and retro-step-up shears except that they intersect above the base so that the stress- and strain-rate singularity is now located inside the layer at the depth appropriate to partition the convergent layer into obducted and subducted components (Figs 8i and ii). We refer to the lower segments of the shears as the pro- and retro-step-down shears because they transfer motion downward as opposed to the upward motion across the step-up shears.

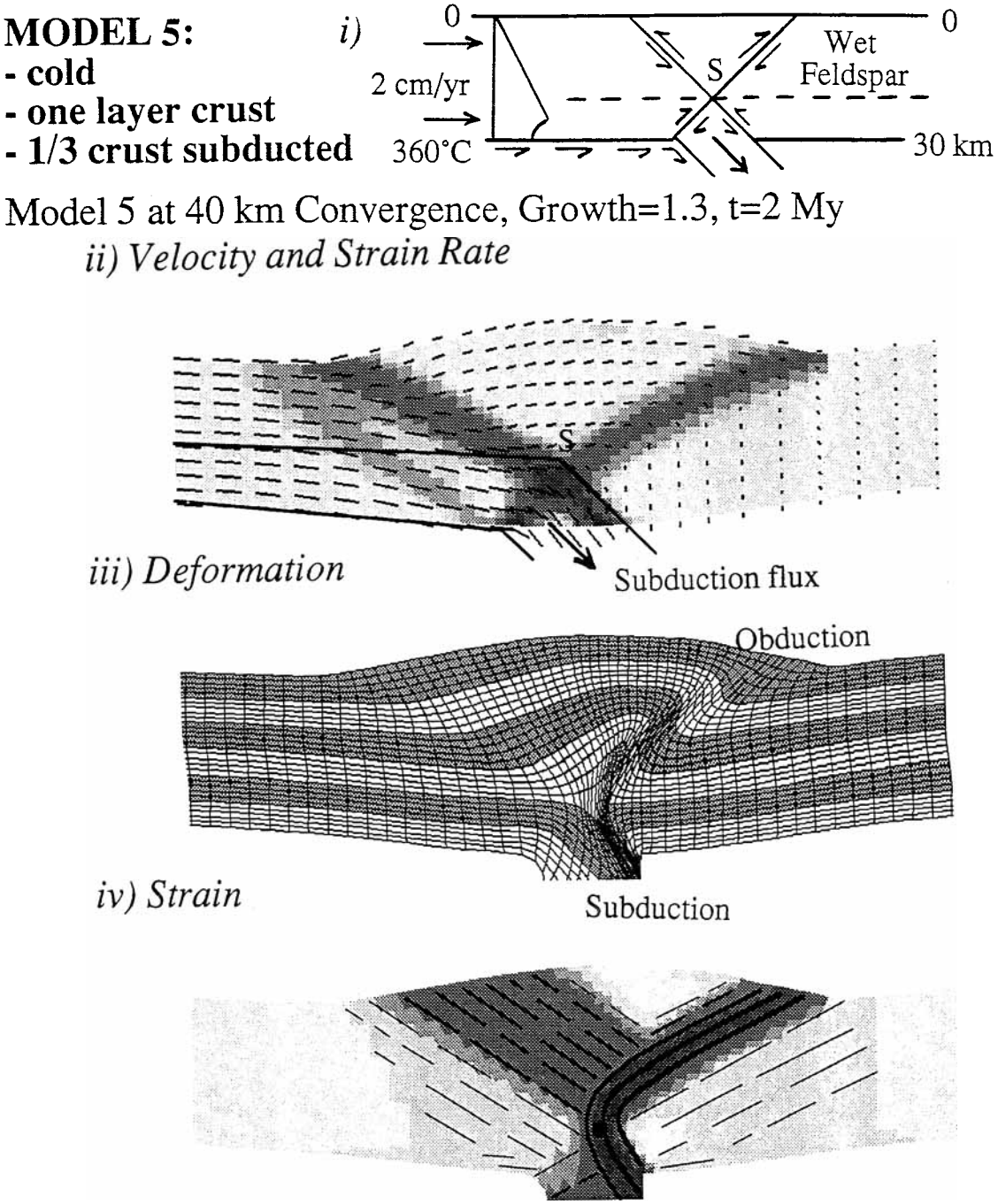

Figure 8. Model 5 results. (i) Model properties and style of deformation. (ii) Velocity and strain rate. Note lower crustal subduction and dynamically determined position of S. (iii) Deformation shown by Lagrangian mesh and grey marker layers. Note style of obduction. (iv) Magnitude of logarithmic strain with stylized-reflectivity fabric overlay. Note region of broad strain occurs above detachment singularity.

Deformation above the singularity is equivalent to that of Model 1, except that the scale is reduced because the singularity depth is only two-thirds of the depth of the layer and hence the amount of material entering the model orogen is reduced. The failure planes dip at the same angle as those of Model 1 and the step-up shears also rotate as the layer thickens (Fig. 8ii). The model develops the same pro-wedge, block uplift and retro-wedge as Model 1.

Below the singularity the deformation (Fig. 8iii) shows the pro-ward crust split into two parts at the level of the singularity. Although both step-down shears have the same strain-rate distributions, only the retro-step-down shear becomes a region of significant deformation and high strain (Fig. 8iv). The step-down shear acts in exactly the same way as the step-up shears when convergence is asymmetric. Fig. 8(iii) gives the impression that the retro-crust is acting as a strong 'indentor' that splits the crust. However, this is a false impression because the deformation is governed by the basal subduction boundary conditions and there is no strength contrast between the pro- and retro-crustal regions in the model.

The strain and inferred seismic-reflectivity patterns after

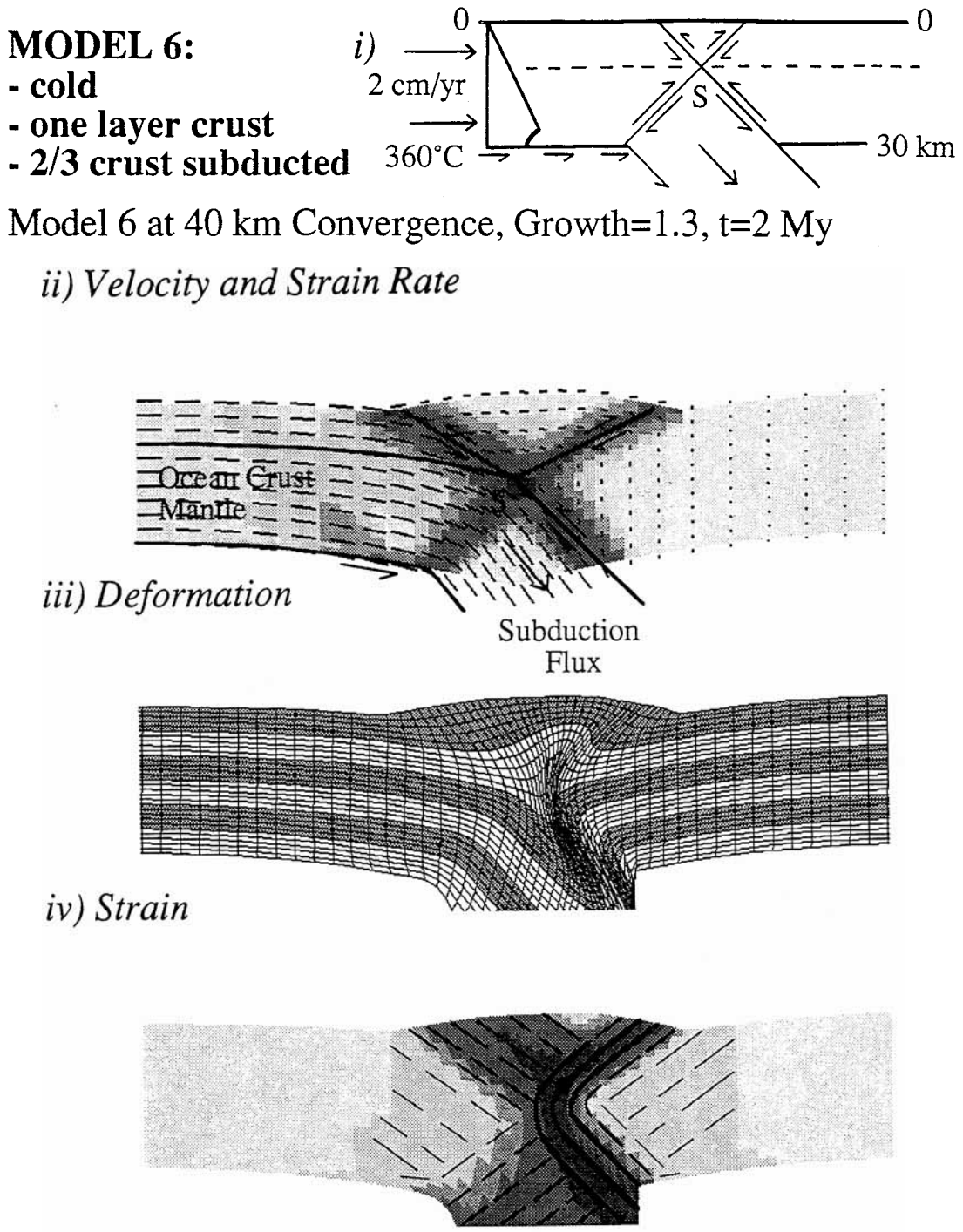

Figure 9. Model 6 results. (i) Model properties and style of deformation. (ii) Velocity and strain rate. Note crustal subduction and dynamically determined position of S. (iii) Deformation shown by Lagrangian mesh and grey marker layers. (iv) Magnitude of logarithmic strain with stylized-seismic-reflectivity fabric overlay.

40 km of convergence (Fig. 8iv) shows the same pro- and retro-wedges as Model 1 but joined to a very highly sheared region in the hanging wall of the subducted crust. In this region the reflectivity fabric dips in the opposite direction to the retro-step-up fabric and the style is reminiscent of various reflectivity 'crocodiles' described by Meissner (1989).

Model 6: cold, one-layer crust, two-thirds crust subducted

Model 6 is the same as Model 5, except that the material flux through the base is larger and corresponds to two-thirds of the convergent mass flux (Fig. 9i). The same dynamic conditions apply to the solution which places the singularity S between obducted and subducted crust close to the surface

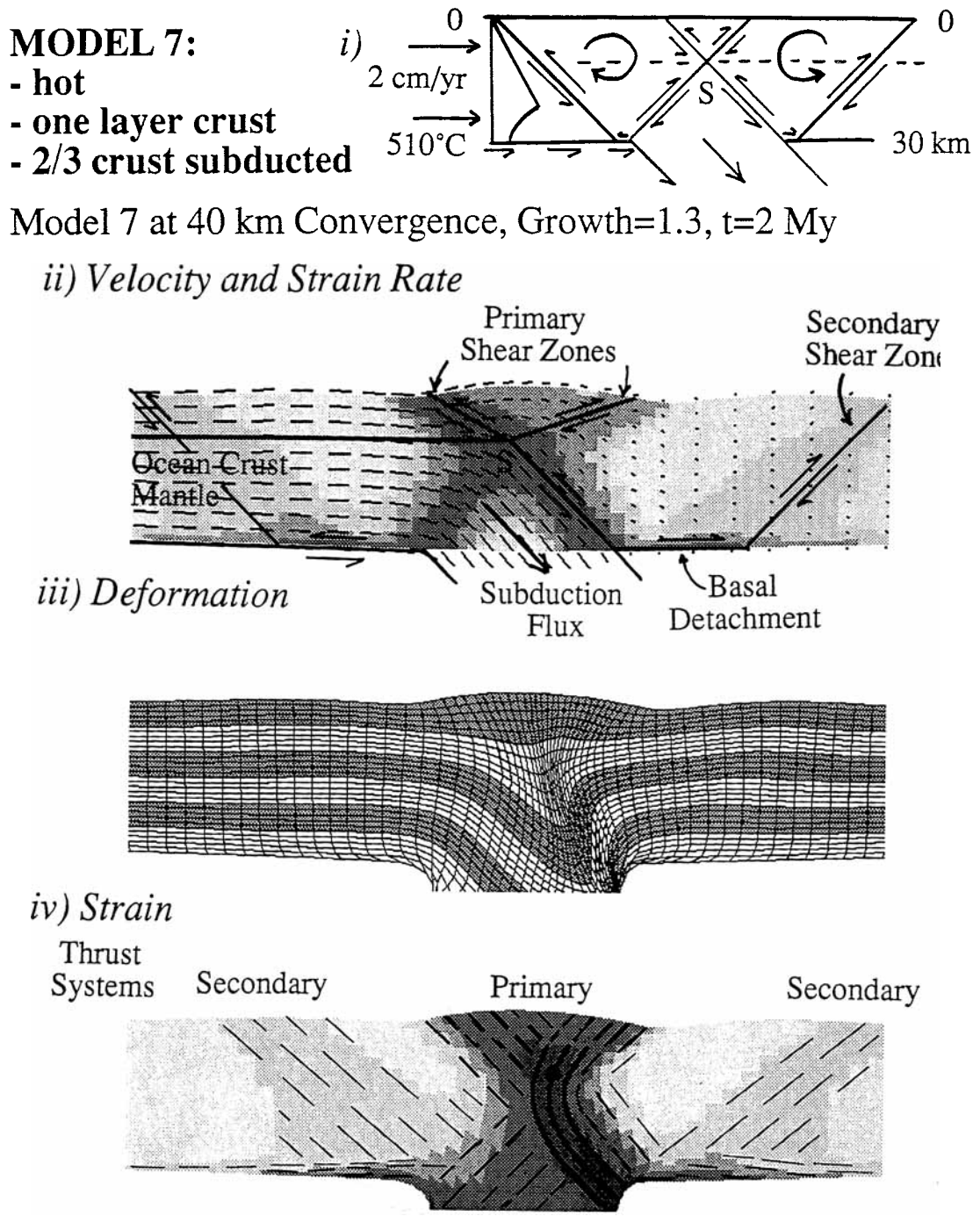

Figure 10. Model 7 results. (i) Model properties and style of deformation. (ii) Velocity and strain rate. Note how the left side can be interpreted to represent subduction of oceanic crust with thick overlying sediments. Note also secondary step-up shear zones related to basal detachment. (iii) Deformation shown by Lagrangian mesh and grey marker layers. Note weakly arched surface above secondary shears which segments the foreland basins. (iv) Magnitude of logarithmic strain with stylized-reflectivity-fabric overlay. Note strain associated with secondary thrust systems.

so that the upper third of the crust corresponds to a small-scale version of Model 1 (Fig. 3b). The two failure planes intersect to create the same cross-deformation mode (Fig. 9ii) that characterized Model 5. It is worth noting that in the limit of total subduction of the pro-ward crust the singularity would be at the surface and the two step-down shears would form an inverted V shape. The retro-crust would remain undeformed beyond the retro-step-down shear zone and there would be no obduction. The style can be pictured by inverting Fig. 8.

The deformation and strain patterns of Model 6 (Figs 9iii and iv) show thickening of a near-surface crustal layer with subduction occurring beneath it. The most highly strained region is the retro-step-down shear, which is deformed as the lower pro-crust is subducted in the footwall. Only small upper level pro- and retro-wedges form because two-thirds

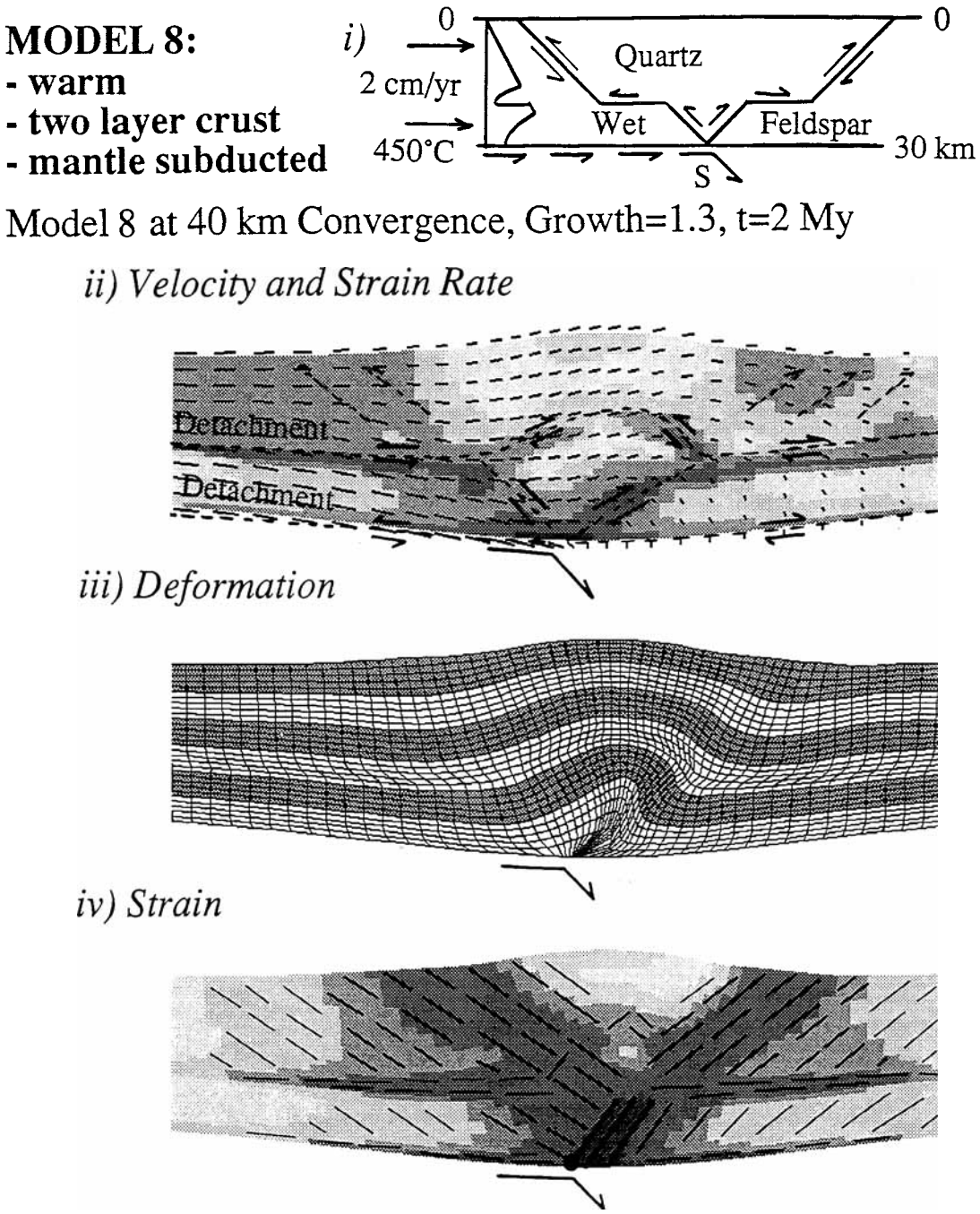

Figure 11. Model 8 results. (i) Model properties and style of deformation. Note intracrustal detachment at base of crustal layer controlled by quartz rheology. (ii) Velocity and strain rate. (iii) Deformation shown by Lagrangian mesh and grey marker layers. Note simple shear at base of quartz dominated crustal layer. (iv) Magnitude of logarithmic strain with stylized-reflectivity fabric overlay. Note partitioning of strain between step-up shears and subhorizontal detachments.

of the convergent mass flux is subducted. Subduction removes incoming crustal material and so plays a similar part to that of denudation in Model 4. The inferred seismic reflectivity pattern contains a 'crocodile' but at a higher level in the crust than in Model 5.

Model 7: hot, one-layer crust, two-thirds crust subducted

Model 7 is the same as Model 6 except that the geothermal gradient is higher and the base is a relatively weak viscous layer (Fig. 10i). Shearing is no longer confined to the crossed shear zones that intersect at the singularity. After only 40 km of convergence the lower crust has detached from its base in both the pro- and retro-directions and two secondary external step-up shear zones couple this deformation to the surface (Fig. 10ii). The zones between the external and central shears remain regions of low-shear-strain rate which flexurally subside while uplift occurs in the hanging wall of the external shear (Fig. 10iii).

The strain distribution and inferred seismic-reflectivity

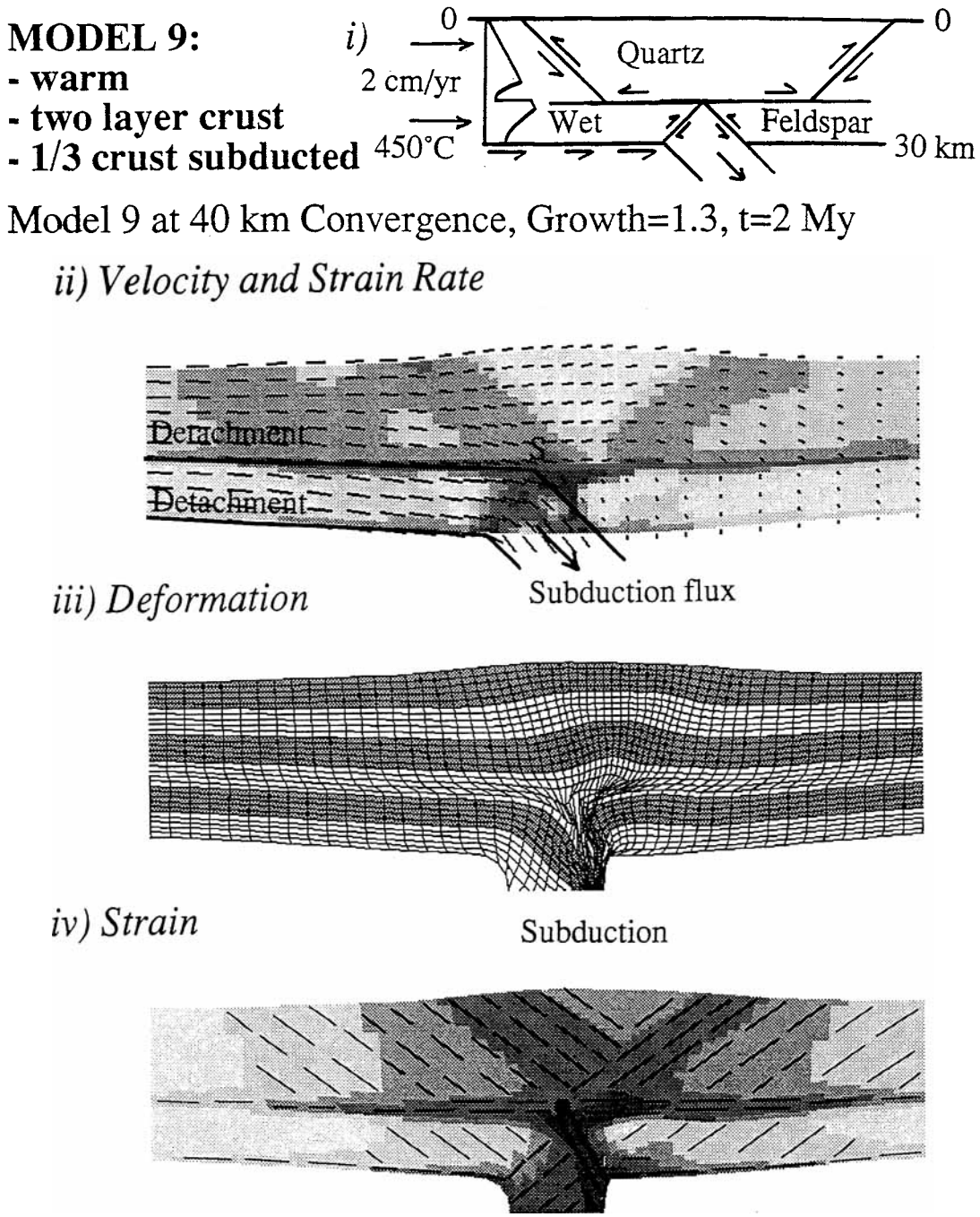

Figure 12. Model 9 results. (i) Model properties and style of deformation. (ii) Velocity and strain rate. Note high-shear-strain rate on intracrustal detachment and the secondary block uplift that is developing in the upper crustal pro-wedge. (iii) Deformation shown by Lagrangian mesh and grey marker layers. Note weakly developed antiform because little of the lower crust is obducted (compare with Fig. 11iii). (iv) Magnitude of logarithmic strain with stylized-reflectivity fabric overlay. Note partitioning of strain between step-up and step-down shears and subhorizontal detachments.

fabric is like that of Model 6, with the addition of the two external zones of weaker crustal-scale thrusting coupled to the detachment singularity by subhorizontal shears in the lower crust.

Model 7 is an interesting example of nested pro- and retro-thrusting at two levels in the crust, even though there is no upper detachment level dictated by material layering as is in Models 8 and 9. In this instance the small upper crustal orogen is a consequence of the dynamically prescribed location of the singularity (Figs 10i and ii) which, in turn, is forced by the subduction flux.

Model 8: warm, two-layer crust, mantle subducted

Model 8 is the same as Model 2 except that the model crust now has two compositional layers with different mineralogies that control the power-law creep. In the upper 20 km 'wet' quartz is assumed to control creep, whereas the lower

10 km are controlled by the behaviour of 'wet' feldspar as in the previous models (Fig. 11i). The brittle–ductile transition occurs at a lower temperature and lower level of deviatoric stress in 'wet' quartz than in 'wet' feldspar (Ord & Hobbs 1989). For this reason the base of the upper crustal layer in this model is a region of lower effective viscosity than the base of the crust (Fig. 11i) despite its lower temperature. Both regions are, however, sufficiently weak that they act as subhorizontal viscous shear zones (Figs 11ii and iii), which decouple the upper and lower crust, and the lower crust and mantle. The subhorizontal shear zones also couple distinct upper and lower crustal pro- and retro-wedges so that the overall style (Fig. 12) corresponds to two stacked doubly vergent tectonic wedges. Deformation in the upper crustal wedges extends further laterally because these wedges have the weaker base.

The crustal antiform (Fig. 11iii) is similar to that of Model 2 (Fig. 5iii) but the additional mid-crustal shear zone can clearly be seen from the deformed Lagrangian mesh. Note that the sense of shear in the mid-crustal shear zone reverses over the antiform compared with the shear beneath the exterior regions of the pro- and retro-wedges. The velocity and deformation fields (Fig. 11) also imply that lower crustal material from the pro-wedge is carried up the retro-step-up shear zone and becomes incorporated into the upper crustal retro-wedge. From a structural viewpoint this process looks like deformation above a large-scale lower crustal flat-ramp-flat footwall.

The strain field (Fig. 11iv) also forms a characteristic pattern in which thrust deformation within the Coulomb-controlled regions of the crust layers roots in the viscously controlled subhorizontal zones of simple shear. Examples of this behaviour also occur in the other models that have weak subhorizontal shear zones. The associated seismic-reflectivity fabric is inferred to have truncation relationships (Fig. 11iv) that are a consequence of the linked pattern of strain.

Model 9: warm, two-layer crust, one-third crust subducted

Model 9 combines Model 8 with Model 5. The model has the same compositional layering and geothermal gradient as Model 8, but the basal boundary condition is that of Model 5 with a subducted mass flux equal to one-third of the convergent mass flux (Fig. 12i). The basal regions of the 'wet' quartz and 'wet' feldspar layers again act as weak viscous subhorizontal shears or detachments (Fig. 12ii) that couple thrusting in the Coulomb-controlled regions of the two stacked wedges back to the basal boundary condition.

The strain-rate distribution in the upper crust (Fig. 12i) resembles the style of Model 2 (Fig. 5ii) in that the pro- and retro-wedges contain the same secondary step-up shears and transient block uplifts. Fig. 12ii shows one example that is active in the pro-wedge.

The deformation style (Fig. 12iii) is similar to that of Model 8 (Fig. 11iii) except that the antiform is poorly developed because the lower crust is subducted and not ramped up the retro-step-up shear zone. Instead, the lower crustal step-down shear zone (Figs 12iii and iv) creates a highly sheared region in the hanging wall of the subducted lower crust below the singularity S.

The strain distribution is similar to that of Model 8 except for the change in dip of the lower crustal retro-shear zone. In Model 9 the crustal-reflectivity fabric is inferred to form a lower crustal 'crocodile' similar to that of Model 5 (Fig. 8iv). In this example, however, the retro-facing 'jaws' are also complemented by a long horizontal band of reflectivity.

COMPARISON WITH SEISMIC-REFLECTIVITY PATTERNS

The nine different geodynamic models that have been presented represent only a subset of possible models, as is illustrated in Fig. 4. Nevertheless, this subset is sufficiently representative to allow comparisons to be made between models involving subduction basal boundary conditions and actual seismic-reflection profiles, the locations of which are shown on the map of Fig. 13. As it happens, many of the real seismic sections discussed have reflectivity patterns that are like model strain patterns. This suggests that it would be possible to find model parameter values capable of fitting models to other seismic sections if this were the objective. However, no attempt has been made to tailor any individual model to match any specific seismic profile. Instead, we wish to show that the range of reflectivity patterns seen in different seismic sections is similar to the range of strain patterns generated by our geodynamic models. By doing so we establish that the basic processes incorporated into our models are plausibly similar to those processes operating in real compressional orogens.

New England Appalachians

Figure 14(i) shows a structural cross-section through the Bronson Hill Anticlinorium and Connecticut Valley Synclinorium of the New England Appalachians. This is a composite of sections presented by Hatcher (1981) and Ando *et al.* (1984). Fig. 14(ii) shows the pattern of seismic reflectivity observed from an onland traverse of these features by Ando *et al.* (1984) and Fig. 14(iv) shows a subparallel marine seismic-reflection profile on the Long Island Platform 200 km to the SE (Phinney 1986). All sections cross the Appalachian orogen at a high angle to regional strike of the orogen (Fig. 13) and are shown reversed east to west (with respect to the original publications in which they appeared) for easier comparison with model results. The onland structural section most closely resembles the deformation patterns of Model 2 (Figs 14iii), with the oppositely vergent faults on the structural section being analogous to the model pro-wedge and retro-wedge fault patterns. We consider the east-dipping band of reflectivity in Fig. 14(ii) to be the seismic expression of the retro-wedge deformation. It is, however, the amplitude and symmetry of the broad form of the Bronson Hill Anticlinorium (shaded band of Fig. 14i) that provides the best evidence for the model polarity and the strength of basal coupling. The Model 2 antiformal passive marker (Fig. 14iii) best reproduces the observed amplitude; Models 3 and 1 (Figs 7 and 5) are correspondingly too small and too large.

Post-orogenic erosion and extension have also modified the observed structure; the Long Island basin (Fig. 14iv) is one manifestation of extension. The horizontal line at zero km depth in Fig. 14(iii) represents the erosional baseline (sea-level) of the model. If the model was to be eroded to this level, isostatic uplift would return the downflexed base

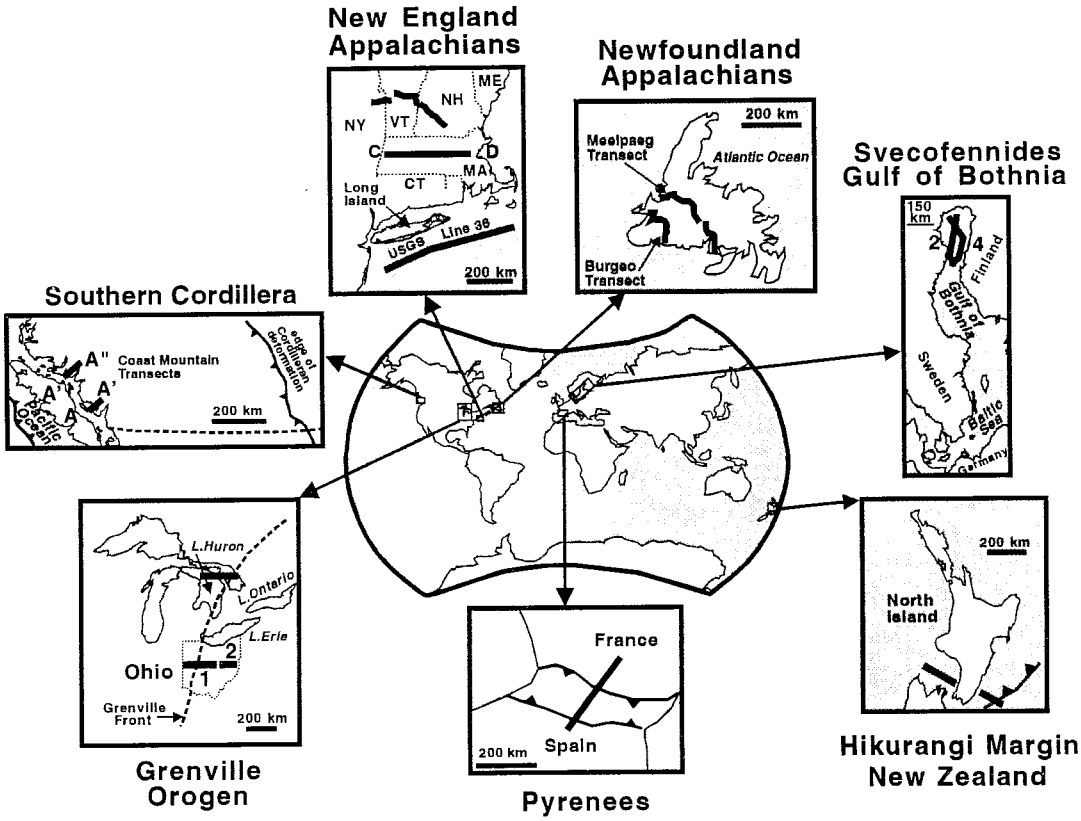

Figure 13. World map showing locations of seismic sections in discussed in Figs 14–20.

of the crust to horizontal and produce a more pronounced uplift of the model antiformal structure.

Although reflectivity of the Long Island platform Line 36 (Fig. 14iv) clearly defines pro- and retro-wedges, it is not clear from the seismic data which is which because the section is largely transparent in the upper 5 s TWT (seconds of two-way traveltime). Marine deep-seismic-reflection data often exhibit upper crustal transparency even though neighbouring terrestrial seismic traverses of comparable features do not (e.g. compare Keen *et al.* 1986 with Quinlan *et al.* 1992). For this reason it is not clear whether the transparent region is actually devoid of reflectivity or whether there is a problem of seismic acquisition and resolution such as discussed by Hurich (1991). Fig. 14(v) shows that the Long Island data can be approximated by Model 3 in which the weak basal layer allows the pro- and retro-wedges to propagate approximately 100 km in either direction from the point of mantle detachment and underthrusting, S. The uplifted wedge of undeformed material in Model 3 is significantly smaller than the unreflective wedge of the Long Island data, suggesting that this lack of reflectivity may be partially an artefact of marine seismic acquisition. The passive marker horizon indicated in Fig. 14(v) is significantly less deformed than its counterpart in Model 2 (Fig. 14iii). In the absence of an identifiable antiform, either Model 2 or 3 would account for the marine seismic data from the Long Island platform. Model 3 would, however, be inferior to Model 2 in its ability to explain the adjacent terrestrial cross-section through the Bronson Hill Anticlinorium.

The model results also closely parallel the simplified conceptual model described by Phinney (1986, Fig. 6) in which the doubly vergent deformation associated with west-dipping subduction is attributed to the Acadian and Alleghanian orogenic episodes.

Pyrenees

Figures 15(i) and 15(ii) show, respectively, unmigrated seismic-reflection data from the ECORS transect across the central Pyrenees and a migrated version of the major reflectors along with an interpretation of the estimated extent of erosion within the orogen (Choukroune *et al.* 1989). The migrated seismic section is very close in form to the strain distribution of Model 5 (Fig. 15iii). The narrow retro-wedge and the much broader zone of pro-wedge deformation calculated for Model 5 are strikingly similar to the narrow NE-verging thrust belt and the broader south-westward verging thrust belt.

Although the geometrical agreement with Model 5 is good, there is no direct evidence for crustal subduction except the vertical offset between the inferred positions of the base of the crust beneath the southern and northern sides of the orogen, respectively. Therefore, Model 1 must be considered as an alternative. Roure *et al.* (1989) believe that subduction beneath the Pyrenees involved only mantle and no lower crust, but the palinspastic restoration of Muñoz (1992) requires some lower crustal subduction. The former interpretation would be most closely analogous to Model 1 and the latter to Model 5. Both of these models

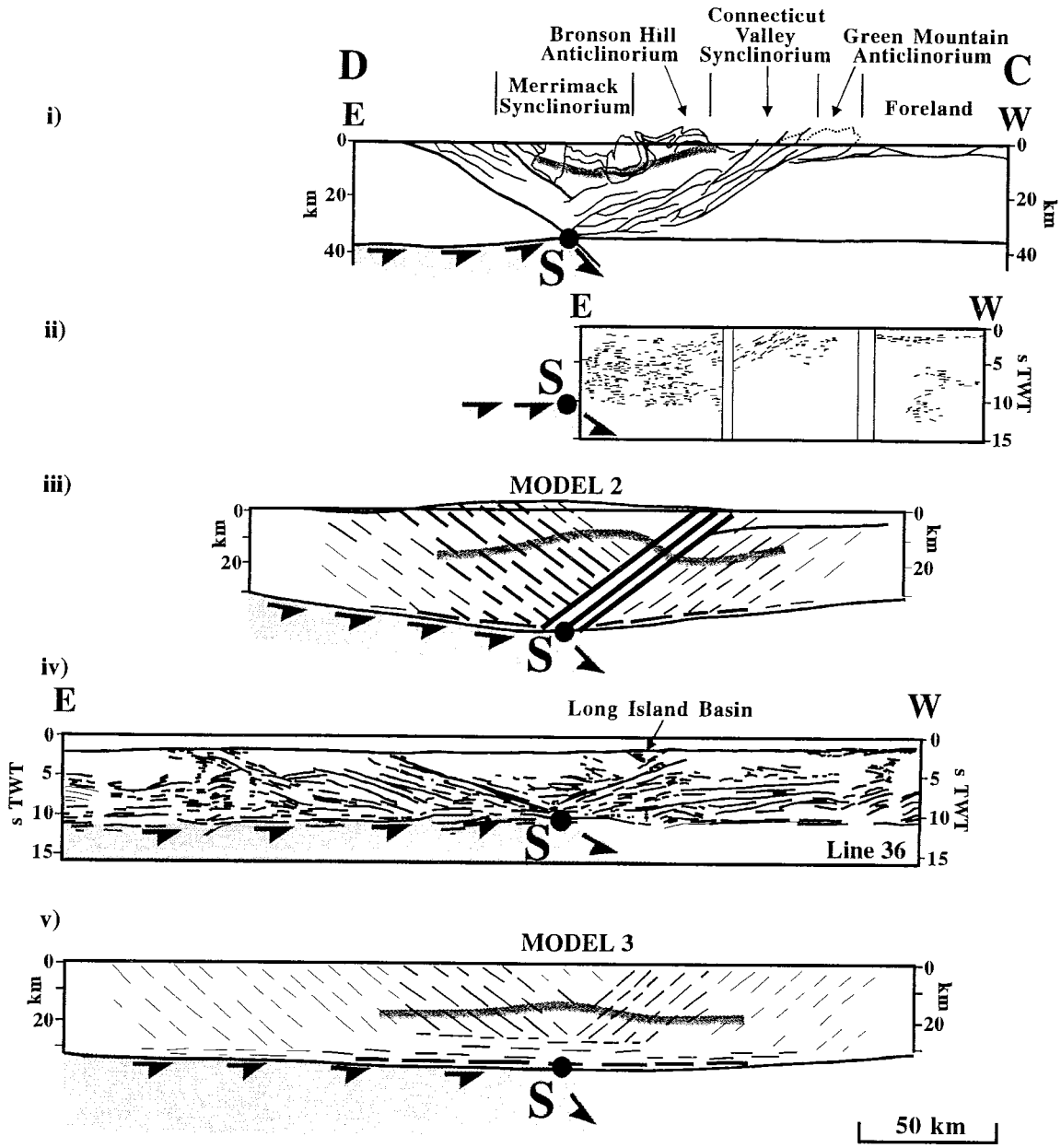

Figure 14. New England Appalachians. (i) Structural cross-section C–D of Fig. 13. Shaded band describes the general form of the Merrimack Synclinorium and Bronson Hill Anticlinorium. (ii) Seismic-reflectivity pattern seen on terrestrial transect from NY to NH shown in Fig. 13 map. (iii) Interpretation of data from top two panels in terms of the strain pattern produced by Model 2 (Fig. 5). Shaded band on this figure emphasizes the model antiform, considered analogous to the Bronson Hill Anticlinorium. (iv) Seismic-reflectivity pattern on USGS Line 36 from the Long Island Platform. Long Island Basin is an extensional feature that does not appear to have significantly modified the overall compressional pattern. (v) Interpretation of the Long Island Platform reflectivity in terms of the strain pattern produced by Model 3 (Fig. 6). Note that data sections are shown reversed from original publications to agree with model polarity. Point S, arrows and shaded region at the base illustrate the interpreted detachment point and sense of subduction of the underlying mantle.

have similar geometry above their singularity points. However, the lateral extent of deformation in our models scales with the depth to the singularity and for this reason Model 5, with its shallower detachment point, provides the better geometrical agreement with the observations. Similar reasoning demonstrates that, without subduction of the lower third of the crust, there would have to be considerably greater crustal thickening for the same amount of convergence. This can be seen by comparing the deformation patterns of Model 1 (Fig. 5) and Model 5 (Fig. 9). The total convergence estimated for the Pyrenees is about 150 km (Muñoz 1992), which would produce a large Model 1 type orogen even when the initial extended configuration and erosion estimates are included. Even the

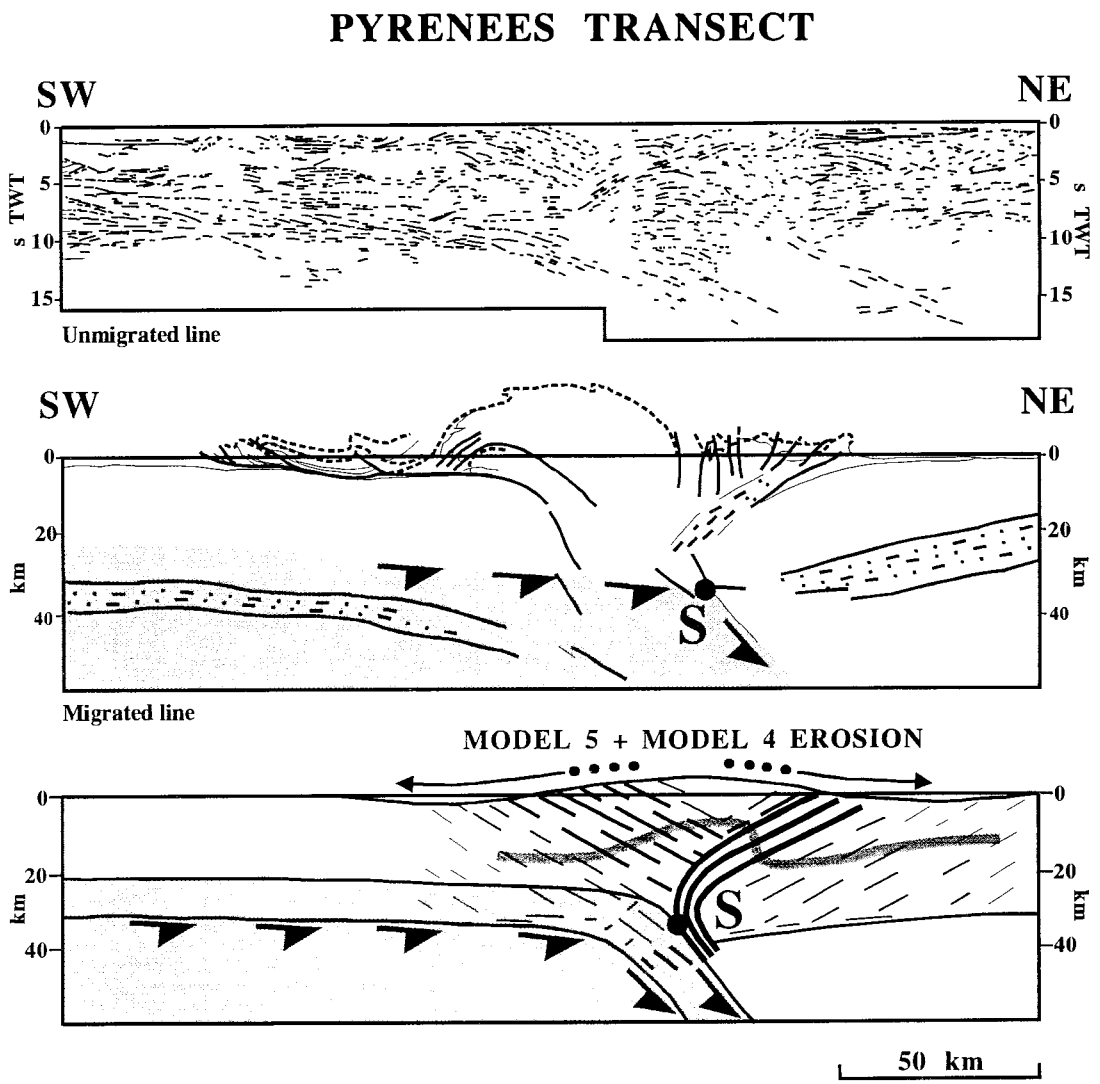

Figure 15. Comparison of inferred seismic-reflectivity fabric and style of crustal antiform from Model 5 (lower panel) with seismic and structural data along a cross-section of the Pyrenees. Note that the mantle reflections on the right side of the unmigrated data (upper panel) become crustal reflections in the migrated section (middle panel). The strongest evidence for the lower crustal subduction seen in the model is the lateral change in the depth of the Moho across the orogen (middle panel). A significant amount of erosion (such as in Model 4) is also required to balance the cross-section (middle panel). Thin-skinned fold-and-thrust belts (middle panel) would be reproduced by the model if a shallow weak detachment was included in the model rheology.

Model 5 style orogen requires as much mass loss from denudation as from subduction if it is to remain no larger than the observed Pyrenees orogen.

The deformed passive horizon, identified by the shaded band in Fig. 15(iii), illustrates the general shape of the crustal antiform which will be further accentuated by syntectonic denudation (Fig. 7iv). The shape of this deformed horizon implies that the location at which rocks have been brought to the surface from mid-crustal depths should lie in the approximate position of the North Pyrenean Fault Zone, in agreement with observation (Muñoz 1992). Greater crustal thickening associated with Model 1 is inconsistent with observations in that it would bring higher grade metamorphic rocks from the lower crust to the surface over too broad a zone.

The subhorizontal reflectivity at about 2 s TWT in the south-western end of the seismic section corresponds to a thin-skinned thrust belt (Choukroune *et al.* 1989). This feature is not predicted by models discussed in this paper because they do not include a shallow rheological contrast corresponding to the sediment–crystalline crust interface. Inclusion of such a contrast (see Fig. 13 of Beaumont *et al.* 1992) results in shallow decoupling in much the same way that the two-layer models, 8 and 9, allow decoupling at mid-crustal depths (Figs 11 and 12). Model 5 does, however, approximately predict the correct flexural subsidence required to produce the form of the Ebro and Aquitaine foreland basins along this transect.

Hikurangi Margin, New Zealand

Figure 16(i) shows a composite seismic profile across the Hikurangi Margin of New Zealand (Stern & Davey 1989;

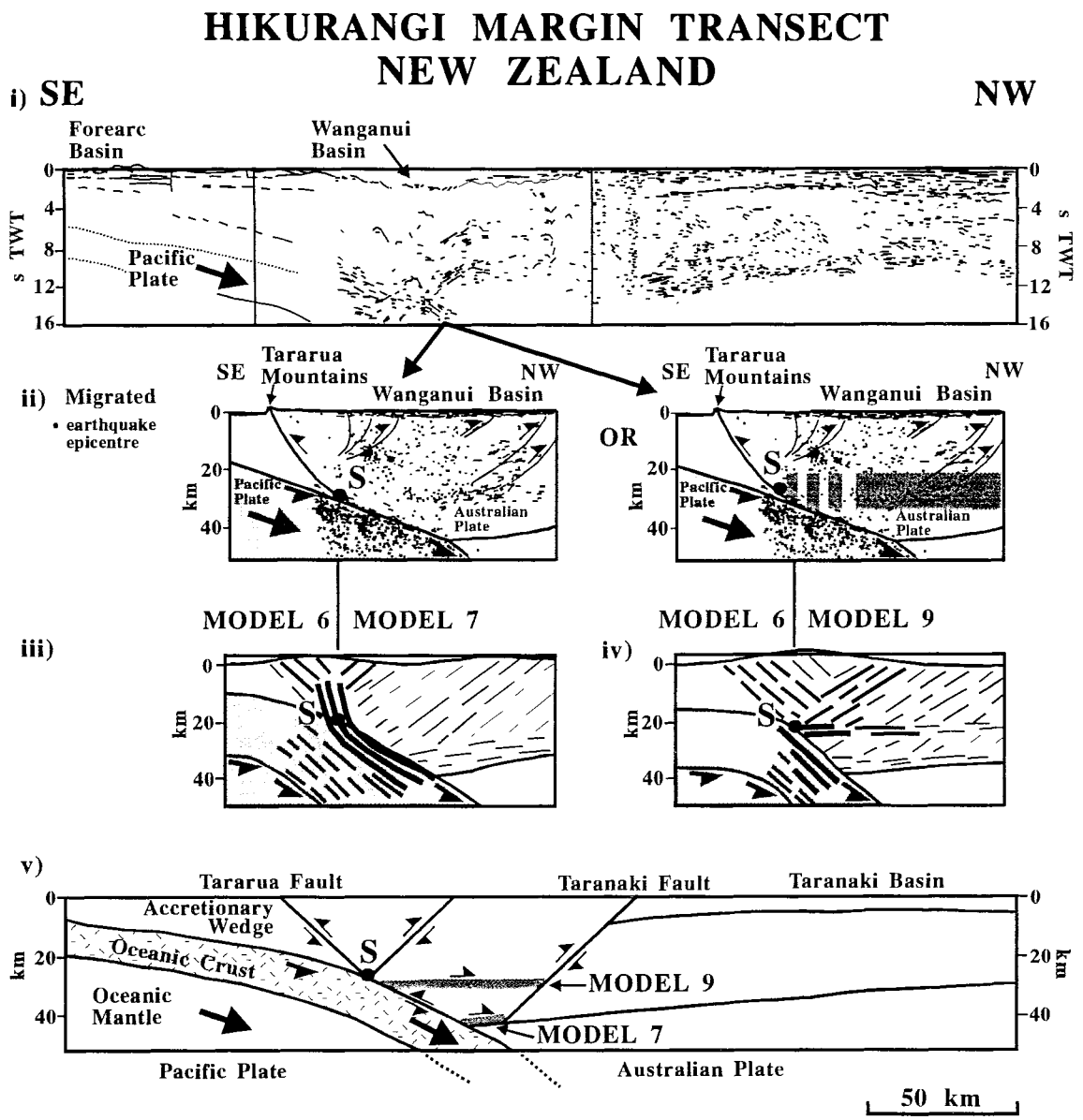

Figure 16. Comparison of the inferred seismic-reflectivity fabric from hybrids of Models 6 and 7 (panel iii) and Models 6 and 9 (panel iv) with seismic-reflection data and earthquake hypocentres from the Hikurangi subduction margin of North Island, New Zealand (panels i and ii). Panel i shows unmigrated data. Panel ii shows migrated data from the central portion of panel i with structural and tectonic interpretations from Stern & Davey (1989) and Stern *et al.* (1992). The most appropriate model interpretation depends on the significance of the mid–lower crustal reflectivity and seismicity in the Australian plate beneath the Wanaganui basin (grey bar, panel ii at right). Panel v shows the two alternative tectonic interpretations from the hybrid models.

Davey & Stern 1990; Stern, Quinlan & Holt 1992) illustrating the geometric relationship of the subducting Pacific plate to the overlying Wanganui and Taranaki basins. Holt & Stern (private communication) have related the development of these basins to the tectonic evolution of the area over the last 32 Myr. We focus on that region underlying the Wanganui basin, a Plio-Pleistocene and younger sedimentary basin.

Figure 16(ii) shows two copies of the same enlarged view of this portion of the composite profile, enhanced with the locations of earthquake epicentres and indications of thrust vergence from first-motion studies and offsets of sedimentary horizons in the basin. The deformation pattern seen for this area is consistent with either of two model hybrids, explained below, both of which have a weaker basal coupling (hotter thermal regime?) beneath the Wanganui basin than further east.

Although we have not presented results for models incorporating lateral variation in mechanical or thermal properties, such variations are to be expected in the real world. For example, at the Hikurangi margin oceanic lithosphere overlain by a thick (about 10 km or more) accretionary wedge is juxtaposed with the continental/arc crust of North Island, New Zealand (Figs 16i and v). Model 6, intended to describe intracontinental subduction in which the lower two-thirds of the crust is subducted, can also be interpreted to approximate the subduction of oceanic crust and mantle detaching from an overlying thick accretionary

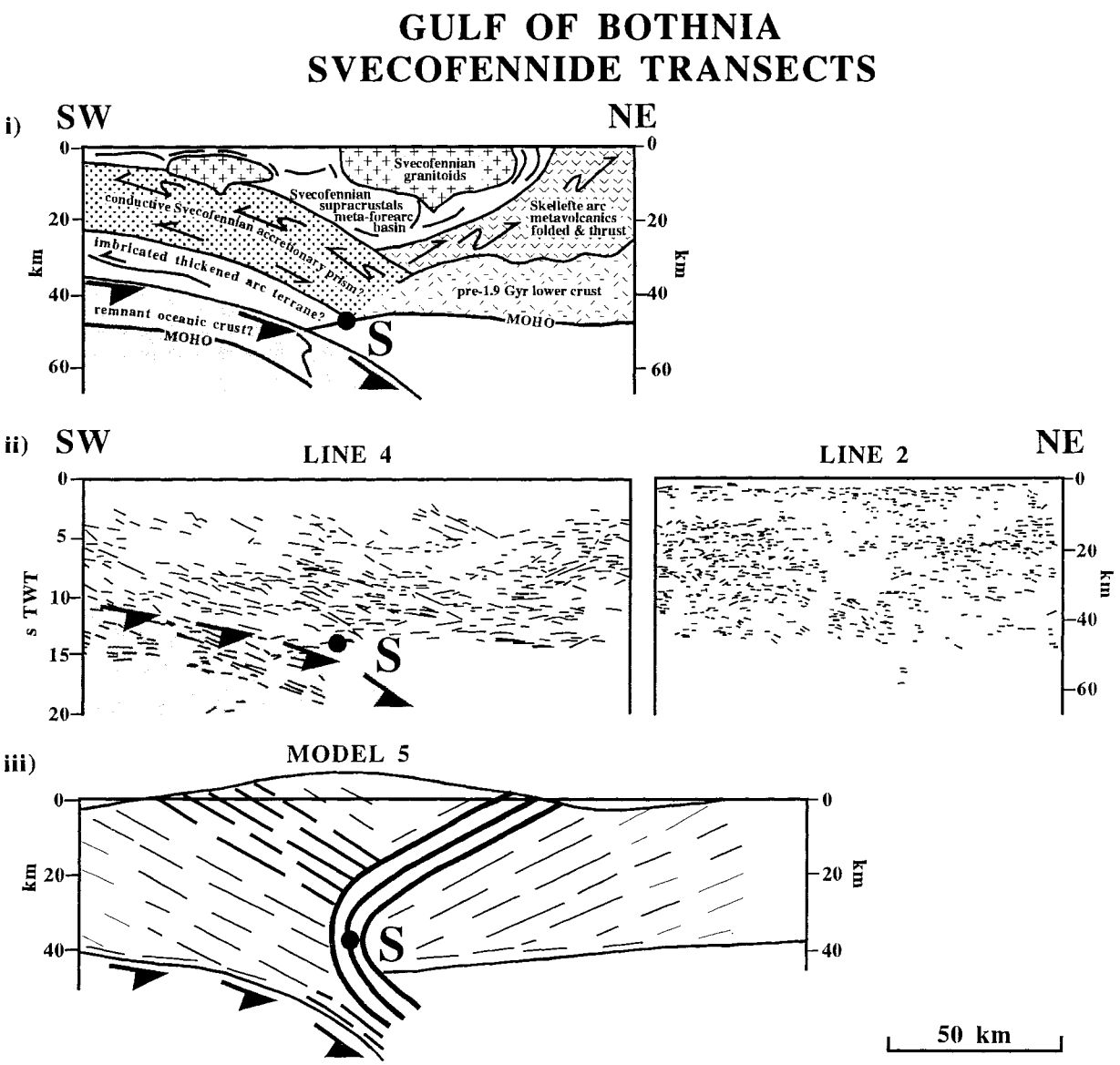

Figure 17. Comparison of the inferred seismic-reflectivity fabric from Model 5 (panel iii) with seismic-reflection data (panel ii) and geological interpretation (panel i) from BABEL lines 2 and 4 in the Gulf of Bothnia. Point S, arrows and shaded region at base of panel ii illustrate the interpreted detachment point and sense of subduction of the oceanic crust beneath the accretionary prism. In this example the crust at the left (panel iii) should be interpreted as oceanic crust with a thick overlying accretionary wedge, similar to the Hikurangi margin (Fig. 16).

prism at point S of Fig. 16(v). Model 6 is therefore appropriate for the Pacific plate side of the Hikurangi margin. However, Model 6 predicts that retro-wedge deformation is confined to the shear zone above the subducting oceanic crust and to the crust above the singularity, a result contrary to the observed crustal-scale seismicity and deformation that extends NW to the Taranaki fault.

Test models have shown that, to a first approximation, it is valid to combine the results of models that have different crustal properties on either side of the singularity to create hybrid models. The results must, however, be rescaled to maintain geometrical and stress continuity in the model crust across the singularity. Figs 16(iii) and 16(iv) show two hybrid models which combine Model 6 with, alternatively, Model 7 or Model 9 NW of the detachment point, S. Models 7 and 9 have a weaker base than Model 6, and so produce the greater observed lateral extent of retro-wedge deformation. A warmer and weaker base is consistent with a warm crust in the vicinity of arc volcanism further north in North Island (Smith, Stern & Reyners 1989). Model 7, which is simply a warmer version of Model 6 (Fig. 4) is acceptable if detachment occurs at the base of the crust. However, if the subhorizontal reflectivity at 30 km depth beneath the basin is interpreted as evidence of shear detachment at this level, the hybrid of Models 6 and 9 which predicts intra-crustal detachment is preferred. These alternative detachment levels are illustrated in Fig. 16(v).

Gulf of Bothnia Svecofennides

Figure 17(ii) shows seismic-reflection data from two transects in the northern Gulf of Bothnia along with a tectonic interpretation by the BABEL Working Group

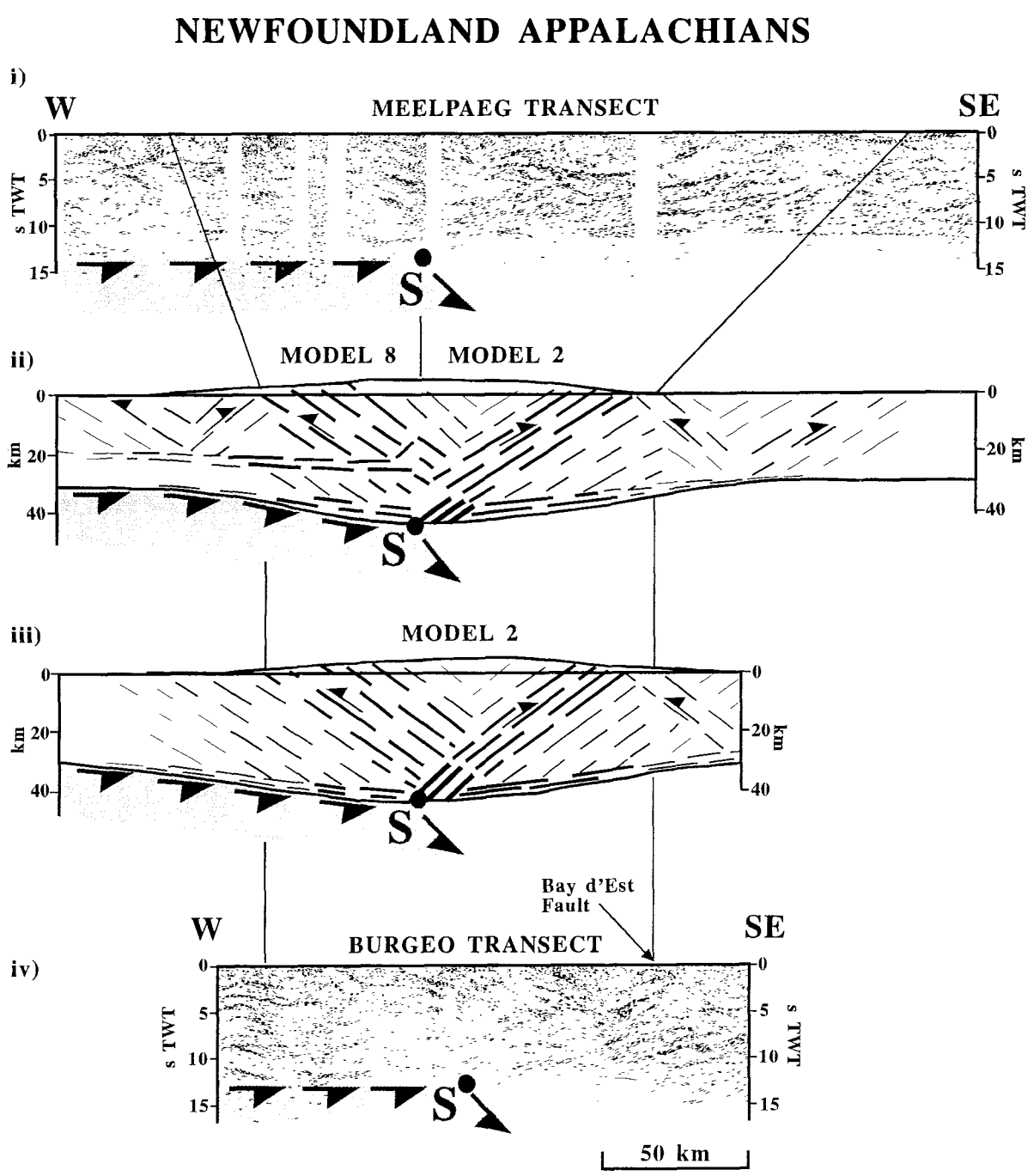

Figure 18. Comparison of the inferred seismic-reflectivity fabric from hybrid of Models 8 and 2 (panel ii) and Model 2 (panel iii) with seismic-reflection data from the Newfoundland Appalachians (panels i and iv). Whether the hybrid Model 8 and 2 is appropriate for the NW end of the section depends on whether or not significance is attached to the lack of reflectivity in the lower crust compared with the upper crust; this may indicate a weak detachment above which westward directed thrusting took place. The Bay d'Est Fault is suggested to be the pro-ward half of a secondary step-up shear zone.

(1991) (Fig. 17i) and a similar interpretation that arises from comparison with Model 5 results (Fig. 17iii). This example provides supporting evidence for the boundary conditions assumed in all models presented in the current paper, i.e. that the doubly vergent deformation is caused by detachment and underthrusting of the lithosphere (BABEL Working Group 1991, 1993). The reflector that extends into the mantle in Line 4 is interpreted to be a remanent slab of oceanic crust, implying subduction with convergence from the SW.

The data and interpretation correspond most closely with Model 5 in which the lower third of the crust is subducted. This model was also used for the Pyrenees. In the present context, however, the pro-wedge is constructed from a deformed accretionary wedge and not a continental margin as in the Pyrenees. From a geological perspective, the Svecofennides transect may be a Proterozoic equivalent of the Hikurangi Margin transect at a more advanced stage of compression.

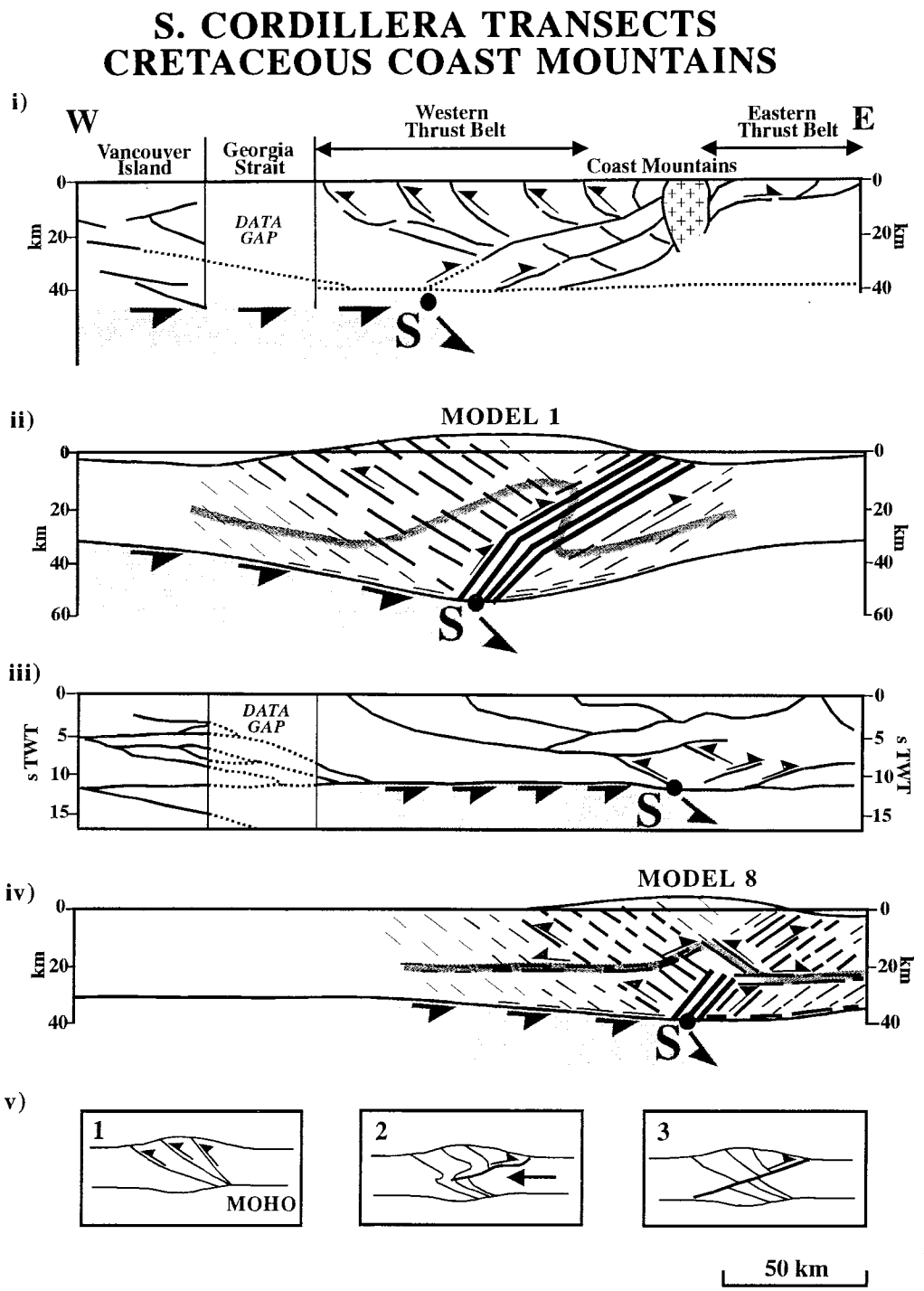

Figure 19. Comparison of the inferred seismic-reflectivity fabric from Model 1 (panel ii) and Model 8 (panel iv) with two interpretations of seismic-reflection and geological data from the Coast Mountains of the Southern Canadian Cordillera (panels i and iii). Note that the models apply only to this small subregion of the total western North American Cordillera. The difference between the two interpretations (panels ii and iv) depends on the significance of the mid-to-lower crustal shear zone in Model 8. Panel v shows the discrete development stages inferred by Varsek *et al.* (1993).

The retro-wedge reflectivity may extend further to the NE than the strain patterns of Model 5. This is not clear from the seismic data of Line 2 (Fig. 17ii), but if true would require a model with a weaker base. A hybrid of Models 5 and 2 or Models 5 and 9 would probably satisfy the observations.

Newfoundland Appalachians

Figures 18(i) and 18(iv) show two seismic profiles across the Newfoundland Appalachians separated by an along-strike distance of about 100 km (Quinlan *et al.* 1992). The Meelpaeg transect (Fig. 18i) crosses the widest portion of

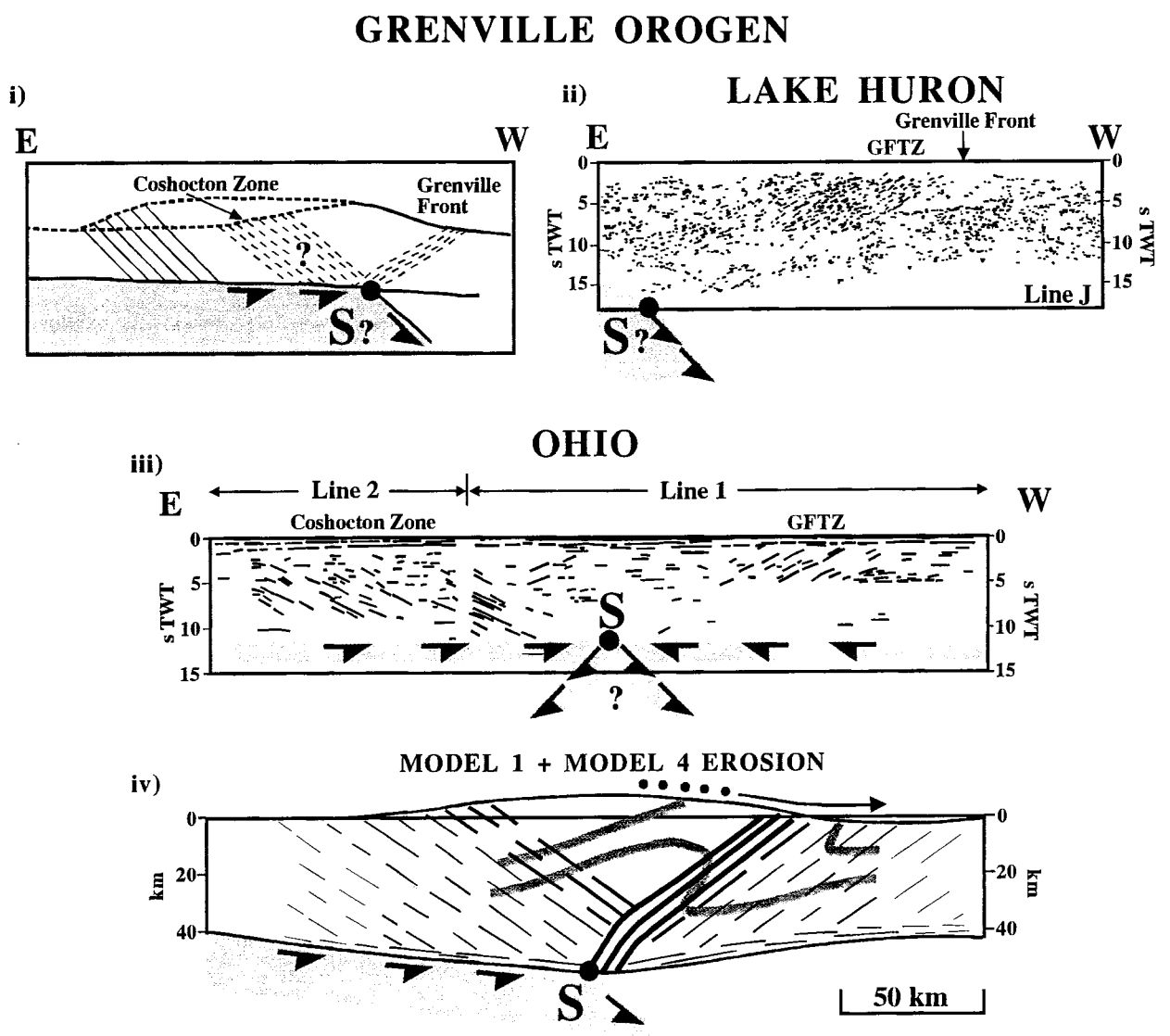

Figure 20. Comparison of the inferred seismic-reflectivity fabric from Model 1 (panel iv) with GLIMPCE (panel ii) and COCORP (panel iii) seismic-reflection data from the western Grenville Orogen in Lake Huron and Ohio, respectively. The model applies to only these small regions of the much larger Grenville Orogen. Note that data sections are reversed with respect to their original publications. The Grenville Front Tectonic Zone (GFTZ) may correspond to a retro-step-up shear zone. The Coshocton Zone may be the corresponding pro-wedge (panels i, iii, iv) or, alternatively, the pro-wedge may be on the other side of the orogen (panel i). The GFTZ in southern Ontario is best explained by a combination of Model 1 retro-wedge growth and a large component of syntectonic denudation as in Model 4. The subduction polarity is not clear from the data.

the orogen in Newfoundland, whereas the Burgeo transect (Fig. 18iv) crosses a narrower portion of the orogen (Fig. 13) to the SW. Both sections show seismic-reflectivity patterns similar to Model 2 in which deformation is distributed across a wide zone with broad pro- and retro-wedge bands of reflectivity. The SE-dipping reflectivity near the SE ends of both the Meelpaeg and Burgeo profiles and the NW-dipping reflectivity near the NW ends of both these profiles can be interpreted as second-order step-up shear zones of the sort generated by Model 2 (Fig. 5ii). What may be the second-order pro-step-up shear on the Burgeo transect coincides with the surface trace of the Bay d'Est fault, the latest movement on which is documented by O'Brien *et al.* (1991) to be south-over-north thrusting with an age of 421 Ma (late mid-Silurian).

Model 2 also generates a subhorizontal shear zone along its weak base. Equivalent shearing may be responsible for the strong Moho reflection seen on the south-eastern end of the Meelpaeg transect (Fig. 18i). A similarly strong Moho reflection is not, however, seen NW of the inferred mantle detachment point, S, on Fig. 18(i) or anywhere on the Burgeo transect (Fig. 18iv).

A partial explanation for this difference in Moho reflectivity, at least along the Meelpaeg transect, may be found in the lateral variation in crustal properties and a different style of deformation NW of the mantle detachment point. There is a general lack of coherent reflectivity in the lower crust beneath the north-western end of the Meelpaeg transect (Fig. 18i). Quinlan *et al.* (1992) note that this absence of lower crustal reflectivity may be related to

acquisition problems in that part of the data set. However, it may also be explained in terms of a Model 2/Model 8 hybrid (Fig. 18ii) in which a mid-crustal detachment in western Newfoundland allows deformation to step up from the basal singularity, transporting material above the detachment and leaving the crust below it largely undeformed. It is not clear from the seismic data of Fig. 18(i) whether this westward propagating detachment occurs within the crust or whether the detachment is best viewed as occurring between crystalline basement and the overlying cover rocks. Stockmal & Waldron (1990; 1991) interpret the seismic data of Fig. 18(i) and 18(iv) to show tens of kilometres of Devonian and/or Acadian westward transport of both basement and sediment cover above autochthonous platform sediments.

The shallow detachment and westward transport interpreted by Stockmal & Waldron (1990; 1991) to occur at about 4 s TWT on western end of the Burgeo transect (Fig. 18iv) may also be decoupled downward to the point of mantle detachment, although the seismic data are less clear on this point. Model 2, therefore, may provide the better approximation to the seismic patterns along all of the Burgeo transect (Fig. 18iii), although either the Model 8 or Model 2 style pro-wedge is allowed by the present data for both transects.

Compressional development of large orogens

The development of large orogens such as the Himalayas, in which shortening is of the order of 1000–2000 km (Molnar & Taponnier 1975), cannot be adequately addressed using Models 1–9 in which compression is 100 km or less. Nevertheless, we suggest that the stages of development of large orogens may be understood in terms of these models provided that consideration is confined to smaller scale components that are limited in time and space. We will consider two examples where this suggestion appears valid: the Cretaceous Coast Mountain Complex of the Canadian Cordillera and the North American Grenville orogen in the vicinity of the Great Lakes.

Coast Mountains Complex, Canadian Cordillera

Figures 19(i) and 19(iii) show two alternative structural interpretations of seismic reflection profiles across the Cretaceous age Coast Mountains. The essential difference involves the manner in which the upper crustal faults are coupled to the singularity at the base of the crust. In Fig. 19(i) (Rushmore & Woodsworth 1991) this coupling is along what we would interpret as east-vergent retro-wedge shears developed in a single-layer crust as in Model 1 (Fig. 19ii). In Fig. 19(iii) (Varsek *et al.* 1993) this coupling is via both east-vergent and west-vergent shears that originate at the base of the crust but feed upward into a mid to lower crustal shear zone such as developed in Model 8 (Fig. 19iv). Note that these alternative interpretations imply different positions for the mantle detachment singularity.

Model 1 results of Fig. 19(ii) are shown after 100 km of convergence, whereas the Model 8 results of Fig. 19(iv) have only 40 km of convergence. We recognize that either of these amounts of convergence is likely to underestimate the actual amount of convergence involved in the formation of the Coast Mountains. The point is that to produce the observed lateral extent of pro-wedge and retro-wedge shears, much greater convergence is necessary in the strongly coupled Model 1 than in the more weakly coupled Model 8. The antiform is more developed in Model 1, therefore, following erosion and isostatic rebound, near-surface material beneath the central Coast Mountains should be of higher metamorphic grade if the structural interpretation of Fig. 19(i) is correct than if the interpretation of Fig. 19(iii) is correct. This effect may, however, be masked by syntectonic plutonism.

No matter which of the interpretations is more reasonable, it appears that the entire package of reflectivity beneath the Coast Mountains can be produced as part of a single tectonic process that follows the termination of oceanic subduction. Varsek *et al.* (1993), in contrast, prefer a two-stage development in which the west-verging thrusts pre-date the east-verging thrusts and are truncated by them (Fig. 19v). Although this may be true, our models show that there is no dynamic necessity for this two-stage process.

It is important to point out that the Cretaceous development of the Coast Mountains is only one stage in the development of the much larger Cordilleran orogen. Brown *et al.* (1993), for example, argue that the Jurassic development of the Selkirk Fan proceeded along lines similar to those we are suggesting for the Coast Mountains. This Jurassic structure was then transported eastward, perhaps by the same compressional stress field responsible for the development of the Coast Mountains Complex and the accretion of the Insular Belt to the west (Gabrielse 1991). Model 8 provides a mechanism for the eastward transport of the Selkirk Fan because crust from west of the singularity ramps up the retro-step-up shear zone, and crust east of the singularity is transported further eastward above the mid-to-lower crustal detachment. This detachment may be analogous to the Monashee décollement (Cook, Varsek & Clowes 1991; Brown *et al.* 1992). If the singularity is located at the westward limit of cratonic North America, the lower crust east of the singularity may be interpreted as transitional crust inherited from Precambrian rifting of the Pacific Ocean.

Grenville Orogen

The Grenville Orogen is another example of a large orogen for which our present models are not strictly applicable if the orogen is viewed in its entirety. Fig. 20(i) is a schematic diagram in which seismic-reflectivity patterns near the Grenville Front are shown as one possible stage in the development of a much larger orogen, the other side of which is difficult to locate precisely. The diagram shows that when a large orogen develops a plateau, the pro-wedge and retro-wedge zones of simple shear deformation may become separated (Willett *et al.* 1993). Therefore, the oppositely dipping reflectivity fabrics need not be adjacent to each other.

Figure 20 shows seismic-reflection data from two crossings of the Grenville Front: one from the GLIMPCE project (Green *et al.* 1988) in Lake Huron (Fig. 20ii) and one from a COCORP transect (Culotta, Pratt & Oliver 1990) farther south in Ohio (Fig. 2iii). Note that these sections are shown reversed left to right from the original publications.

The Lake Huron data show reflectivity of only a single vergence and so, on their own, make it difficult to decide whether these reflectors are pro- or retro-side features. The density of reflectivity, the high grade of surface metamorphic rocks, and evidence of their rapid exhumation (Rivers *et al.* 1989; Haggart *et al.* 1993) within the Grenville Front Tectonic Zone (GFTZ) suggest that the GFTZ may be a retro-wedge whose lateral development is localized by syn-compressional erosion. This denudation was probably focused on the flank of the large Grenville orogen and would not have been complete, as in Model 4 (Fig. 7). Instead, our preferred model is a variation of Model 1 in which some syn-compressional denudation occurs. If pro-wedge reflectivity is not detected SW of the end of the Lake Huron line (Green *et al.* 1988), one interpretation is that the orogen was large enough for the pro- and retro-wedge reflectivity to have become separate as in Fig. 20(i). Alternatively, evidence from the Central Britt domain of the Grenville Orogen in southern Ontario indicates that the interior of the Grenville Orogen extended shortly before or at the same time the GFTZ rocks were exhumed (Jamieson *et al.* 1992; Ketchum *et al.* 1992). This process is compatible with the predictions of models of large orogens (Willett *et al.* 1993) which undergo gravitationally driven extension as the base becomes hotter and weaker. Extension in the interior therefore causes, and coincides with, compression and thrusting in the exterior pro- and retro-wedges.

Despite the evidence for late stage, syn-orogenic extension of the Grenville Orogen in southern Ontario, the other data set from further to the south in Ohio shows reflectivity patterns of two different vergences such as predicted by the modified form of Model 1 (Fig. 20iv). There is little indication in the seismic data as to whether the Coshocton Zone reflectivity (Culotta *et al.* 1990) has been transported in the direction of vergence of the GFTZ reflectivity or vice versa. These reflectivity patterns are buried beneath flat-lying Palaeozoic sediments of the Appalachian foreland indicated by the subhorizontal reflectivity in the upper 1–2 s TWT of Fig. 20(iii) (Culotta *et al.* 1990) and so direct sampling of the rocks for characteristics such as metamorphic grade is difficult. For that matter, there is no direct evidence that the Coshocton and GFTZ reflectivity patterns formed coevally. We show the Coshocton reflectivity as equivalent to pro-wedge deformation and the GFTZ as equivalent to retro-wedge, but acknowledge that this is not well constrained.

DISCUSSION AND CONCLUSIONS

It is clear that seismic profiles from many compressional orogens contain reflectivity patterns consistent with those inferred from our finite-element models on the basis that strain and reflectivity patterns correlate. Fig. 21 is a schematic diagram illustrating the range of features that can be produced from our existing models depending on the

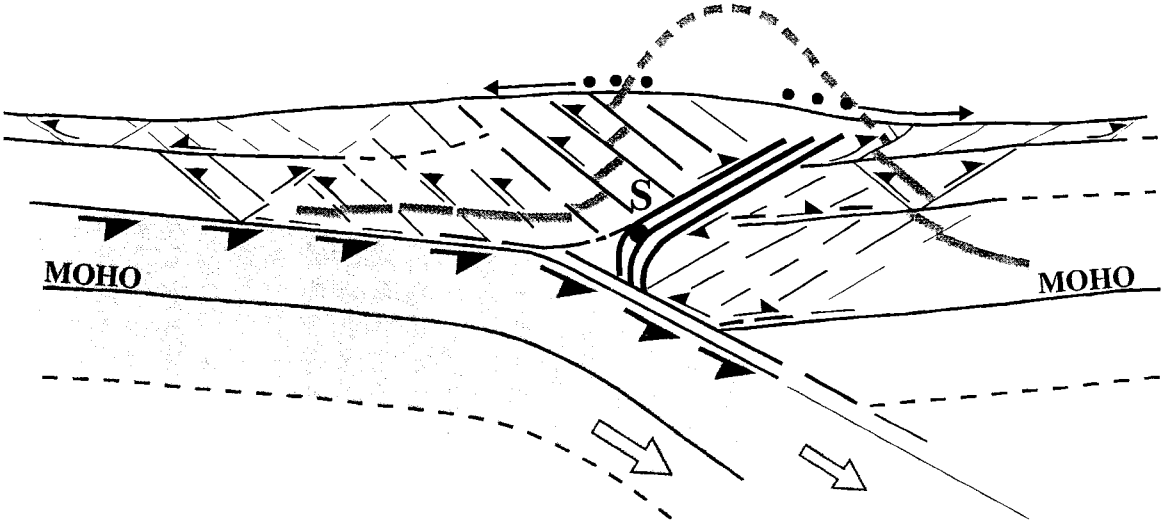

Figure 21. Schematic diagram illustrating the range of deformation styles and inferred seismic-reflectivity fabric anticipated for a small compressional orogen where deformation is fundamentally controlled by subduction of the underlying mantle lithosphere. This figure is a composite of the many styles generated by Models 1–9 and also incorporates, conceptually, effects such as lateral variation in crustal rheology not specifically addressed in these models. Such lateral variation could be the result of different thermal regimes or contrasting petrological structure between the two sides of the compressional orogen. The left side of the section has lower crustal subduction beneath a weak detachment as well as a higher level detachment at the crust–sediment interface. Both these detachments are shown as generating secondary step-up structures that link back to the fundamental detachment point S. The right side of the section shows the effects of a cooler thermal regime in which the crust and mantle are more strongly coupled. As well as this lateral strength difference at Moho depth the right side of the section includes a mid-crustal detachment weaker than that at the Moho. This allows deformation to propagate to greater distances in the upper than lower crust, similar to a flat-ramp-flat style of deformation. As with the left side of the section, a detachment exists at the crust–sediment interface allowing deformation to propagate still further in the sediment layer. The antiformal development of the pro-wedge is amplified by denudation, implied by the broken line above the surface. Parts of the stippled antiformal marker are shown dismembered by small offset pro- and retro-ward thrusting. This emphasizes that reflectivity generated by pre-existing lithological boundaries may be transported by the overall deformation pattern within the compressional system. If such reflectivity is not overprinted by compressional strain it will remain and produce more complicated patterns than those due purely to mechanisms described by our models.

strength of coupling across the crust–mantle boundary, the levels of detachment within the crust, and the amount of crust, if any, that is subducted along with the mantle. This diagram shows not only possible reflective shear zones and faults produced as a consequence of orogenic deformation, but also pre-existing horizons that were transported and disrupted by this deformation (e.g. the stippled antiformal feature was horizontal before deformation). Such pre-existing features may or may not be discernible seismically. Examination of the cumulative strain calculated from Models 1–9 (Figs 2, 5–12) shows regions that are advected in the overall deformation pattern without accumulating significant additional strain. Any pre-existing reflectivity that occurs within such regions would be expected to survive compressional overprinting and so be superimposed on the reflectivity generated during the final stage of compression. In contrast, pre-existing reflectivity that is caught up in areas of high strain may be overprinted to an extent that it is no longer discernible as a separate pattern.

We have deliberately chosen our examples from orogens in which the reflectivity patterns closely resemble the strain patterns predicted by our models and believe that these are examples of orogens in which seismic reflectivity is dominantly the result of strain induced at the later stages of compressional deformation. Whether or not seismic reflection data can constrain multiple phases of tectonic activity depends on the extent to which these phases have obscured each other. We have not as yet considered models in which extension is superimposed on orogenic compression and so do not wish to speculate on what the effects of such superposition might be. However, it may be worth noting that in areas where some amount of post-orogenic extension is demonstrable (e.g. New England Appalachians, Fig. 14), the overall reflectivity pattern retains the character of the compressional models.

The Swiss Alps (e.g. Butler 1990; Pfiffner *et al.* 1990; Hollinger & Kissling 1992) provide a clear example of an orogen in which seismic-reflectivity patterns are preserved from multiple phases of tectonic evolution. We are convinced that the first-order structure of the central Alps can be explained by the transition from oceanic subduction to collision accompanied by a crustal response that is broadly like Fig. 21 or Model 5 (Fig. 8). We will use the same methods as in this paper to elaborate on the geodynamic evolution of the Alps in a future paper.

Our geodynamic models are at at an early stage of development and much work remains to be done in refining and extending their capabilities. The models assume plane strain and so are not strictly applicable to orogens involving transpressional deformation. It might be speculated that our model results would be applicable in such orogens if the normal component of convergence dominated the tangential component. However, a definite examination of such situations must await the development of fully 3-D finite-element models. Models involving lateral compositional, thermal and mechanical heterogeneity, greater degrees of compression and more complicated tectonic histories, such as time-varying convergence, reversal of subduction polarity or migration of the detachment singularity, are obvious extensions to the basic model that can and will be addressed within the limitations of plane-strain approximations. In addition, basal boundary conditions other than subduction must be investigated.

Because the range of model parameters examined has not been exhaustive, the range of deformational styles predicted by our models is not exhaustive. We do not claim that other deformational processes cannot occur, nor that reflectivity patterns more complicated than those predicted in this paper cannot result from compressional orogenesis. Despite these limitations, the similarity between model results and observed reflectivity patterns suggests that the tectonic evolution of many small orogens may have involved processes similar to those controlling model evolution. In addition, it appears likely that aspects of large orogens can be understood in terms of these models if attention is restricted to temporally and spatially discrete components of these large orogens.

At their present stage of development, the models are best thought of as providing additional, and not otherwse obtainable, information that can help to unravel the evolutionary history of compressional orogens by providing a simple dynamic framework within which to interpret the various geological, geophysical and geochemical indicators of this history.

ACKNOWLEDGMENTS

We thank P. Cawood and C. Hurich for useful comments on an early version of the manuscript. P. Fullsack, S. Willett and J. Hamilton contributed significantly to the development of the numerical models. T. Stern provided advice on the New Zealand seismic data. Funding for this work was through grants to the authors from the Canadian Natural Sciences and Engineering Research Council and from the Canadian LITHOPROBE program. LITHOPROBE contribution number 463.

REFERENCES

Ando, C.J., Czuchra, B.L., Klemperer, S.L., Brown, L.D., Cheadle, M.J., Cook, F.A., Oliver, J.A., Kaufman, S., Walsh, T., Thompson, J.B., Lyons, J.B., & Rosenfeld, J.L., 1984. Crustal profile of mountain belt: COCORP deep seismic reflection profiling in New England Appalachians and implications for architecture of convergent mountain chains, *Am. Assoc. Petrol. Geol. Bull.*, **68**, 819–837.

BABEL Working Group, 1991. Evidence for early Proterozoic plate tectonics from seismic reflection profiles in the Baltic shield, *Nature*, **348**, 34–38.

BABEL Working Group, 1993. Integrated seismic studies of the Baltic shield using data from the Gulf of Bothnia region, *Geophys. J. Int.*, **112**, 305–324.

Beaumont, C., Fullsack, P. & Hamilton, J., 1994. Styles of crustal deformation caused by subduction of the underlying mantle, *Tectonophysics*, in press.

Beaumont, C., Fullsack, P., Hamilton, J. & Willett, S., 1992. Preliminary results from a mechanical model of the tectonics of compressive crustal deformation, in *Alberta Basement Transect Report, Workshop Report 28*, pp. 27–61, ed. Ross, G.M., LITHOPROBE Secretariat, University of British Columbia, Vancouver.

Brown, R.L., Carr, S.D., Johnson, B.J., Coleman, V.J., Cook, F.A., & Varsek, J.L., 1992. The Monashee decollement of the southern Canadian Cordillera: a crustal-scale shear zone linking the Rocky Mountain Foreland to the lower crust beneath accreted terranes, in *Thrust Tectonics*, pp. 357–364, ed. McClay, K.R., Chapman & Hall, London.

Brown, R., Beaumont, C., & Willett, S. Comparison of the Selkirk Fan Structure with mechanical models: implications for palinspastic reconstructions of the Southern Canadian Cordillera, *Geology*, **21,** 1015–1018.

Butler, R.W.H., 1990. Notes on crustal balancing along the Alpine segment of the European Geotraverse, in *Fifth European Geotraverse Workshop, Data Compilation and Synoptic Interpretation*, pp. 262–276, eds Freeman, R., Giese, P. & Mueller, S., European Science Foundation, Strasbourg.

Choukroune, P. & ECORS Team, 1989. The ECORS Pyrenean deep seismic profile reflection data and the overall structure of an orogenic belt, *Tectonics*, **8,** 23–39.

Cook, F.A., Varsek, J.L. & Clowes, R.M., 1991. Lithoprobe reflection transect of southwestern Canada: Mesozoic thrust and fold belt to mid-ocean ridge, in *Continental Lithosphere: Deep Seismic Reflections, Geodynamics Series*, Vol. 22, pp. 247–355, eds Meissner, R., Brown, L., Durbaum, H.-J., Franke, W., Fuchs, K. & Seiferet, F., Am. geophys. Un., Washington, DC.

Culotta, R.C., Pratt, T., & Oliver, J., 1990. A tale of two sutures: COCORP's deep seismic surveys of the Grenville province in the eastern U.S. midcontinent, *Geology*, **18,** 646–649.

Dahlen, F.A., 1984. Noncohesive critical Coulomb wedges: an exact solution, *J. geophys. Res.*, **89,** 10 125–10 133.

Davey, F.J. & Stern, T.A., 1990. Crustal seismic observations across the convergent plate boundary, North Island, New Zealand, *Tectonophysics*, **173,** 283–296.

Fullsack, P., 1994. An arbitrary Lagrangian–Eulerian formulation for creeping flows and its application in tectonic models, *Geophys. J. Int.*, submitted.

Gabrielse, H., 1991. Structural styles, in *Geology of the Cordilleran Orogen in Canada, Geology of Canada*, Vol. 4, pp. 571–675, eds Gabrielse, H. & Yorath, C.J., Geological Survey of Canada, Ottawa, Ontario.

Green, A.G., Milkereit, B., Davidson, A., Spencer, C., Hutchinson, D.R., Cannon, M.W., Lee, M.W., Agena, W.F., Behrendt, J.C., & Hinze, W. J., 1988. Crustal structure of the Grenville Front and adjacent terranes, *Geology*, **16,** 788–792.

Haggart, M.J., Jamieson, R.A., Reynolds, P.H., Krogh, T.E., Beaumont, C. & Culshaw, N. G., 1993. Last gasp of the Grenville Orogeny—thermochronology of the Grenville Front Tectonic Zone near Killarney, Ontatio, *J. Geol.*, **101,** 575–589.

Hall, J., 1989. Base of the crust: seismological expression, geological evolution and basin controls, in *Extensional Tectonics of the North Atlantic, Am. Assoc. Petrol. Geol. Mem.*, **46,** 41–52, eds Tankard, A. & Balkwill, H., Am. Assoc. Petrol. Geol., Tulsa, Oklahoma.

Hatcher, R.D., Jr, 1981. Thrusts and nappes in the North American Appalachian orogen, in *Thrust and Nappe Tectonics*, pp. 491–499, eds McClay, K.R. & Price, N.J., Spec. Publ. Geol. Soc. Lond. No. 9.

Hollinger, K. & Kissling, E., 1992. Gravity interpretation of a unified 2-D acoustic image of the central Alpine collision zone, *Geophys. J. Int.*, **111,** 213–225.

Holt, W.E. & Stern, T.A., 1994. Subduction, platform subsidence and foreland thrusting: the late Tertiary development of Taranaki Basin, New Zealand, in press.

Huiqi, L., McClay, K.R., & Powell, D., 1992. Physical models of thrust wedges, in *Thrust Tectonics*, pp. 71–81, ed. McClay, K. R., Chapman & Hall, London.

Hurich, C.A., 1991. Source-generated noise in marine seismic profiles: the limits of reflection detectability in the upper crust, in *Continental Lithosphere: Deep Seismic Reflections, Geodynamics Series*, Vol. 22, pp. 443–450, eds Meissner, R., Brown, L., Durbaum, H.-J., Franke, W., Fuchs, K. & Seiferet, F., Am. geophys. Un., Washington, DC.

Hurich, C.A. & Smithson, S.B., 1987. Compositional variation and the origin of deep crustal reflections, *Earth Planet. Sci. Lett.*, **85,** 416–426.

Hurich, C.A., Smithson, S.B., Fountain, D.M. & Humphreys, M.C., 1985. Seismic evidence of mylonite reflectivity and deep structure in the Kettle dome metamorphic core complex, Washington, *Geology*, **13,** 577–580.

Jamieson, R.A., Culshaw, N.G., Wodicka, N., Corrigan, D. & Ketchum, J.W.F., 1992. Timing and tectonic setting of Grenvillian metamorphism—constraints from a transect along Georgian Bay, Ontario. *J. metamorphic Geol.*, 10, 21–332.

Jaoul, O., Tullis, J. & Kronenberg, A.K., 1984. The effect of varying water contents on the creep behaviour of Heavitree quartzite, *J. geophys. Res.*, **89,** 4298–4312.

Keen, C.E., Keen, M.J., Nichols, B., Reid, I., Stockmal, G.S., Colman-Sadd, S.P., O'Brien, S.J., Miller, H., Quinlan, G., Williams, H., & Wright, J., 1986. A deep seismic reflection profile across the northern Appalachians, *Geology*, **14,** 141–145.

Ketchum, J.W.F., Culshaw, N.G., Jamieson, R.A. & Heaman, L.M., 1992. Structure, metamorphism and geochronology of high grade gneiss within and adjacent to the Central Britt Shear Zone, Central Gneiss Belt, Southwestern Grenville Province, in *Programme with Abstracts*, Vol. 17, Geological Association of Canada, p. A57, Wolfville, Nova Scotia, Canada.

Klemperer, S.L. & the BIRPS Group, 1987. Reflectivity of the crystalline crust: hypotheses and test, *Geophys. J. R. astr. Soc.*, **89,** 217–222.

Litak, R.K., Marchant, R.H., Brown, L.D., Pfiffner, O.A. & Hauser, E.C., 1991. Correlating crustal reflections with geologic outcrops: seismic modelling results from the southwestern USA and the Swiss Alps, in *Continental Lithosphere: Deep Seismic Reflections, Geodynamics Series*, Vol. 22, pp. 299–305, eds Meissner, R., Brown, L., Durbaum, H.-J., Franke, W., Fuchs, K. & Seiferet, F., Am. geophys. Un., Washington, DC.

Malavieille, J., 1984. Modelisation experimentale des chevauchements imbriques: application aux chaines des montagnes, *Bull. Soc. Géol. Fr.*, **26,** 129–138.

Meissner, R., 1989. Rupture, creep, lamellae and crocodiles, *Terra Nova*, **1,** 17–28.

Meissner, R., Brown, L., Durbaum, H.-J., Franke, W., Fuchs K., & Seiferet, F., 1991. *Continental Lithosphere: Deep Seismic Reflections, Geodynamics Series*, Vol. 22, Am. geophys. Un., Washington, DC.

Molnar, P. & Tapponier, P., 1975. Cenozoic tectonics of Asia: effects of continental collision, *Science*, **189,** 419–426.

Mooney, W.D. & Brocher, T.M., 1987. Coincident seismic reflection/refraction studies of the continental lithosphere: a global review, *Rev. Geophys.*, **25,** 723–742.

Muñoz, J.A., 1992. Evolution of a continental collision belt: ECORS-Pyrenees crustal balanced cross-section, in *Thrust Tectonics*, pp. 235–246, ed. McClay, K.R., Chapman & Hall, London.

O'Brien, S.J., O'Brien, B.H., O'Driscoll, C.F., Dunning, G.R., Holdsworth, R.E. & Tucker, R., 1991. Silurian orogenesis and the NW limit of Avalonian rocks in the Hermitage Flexure, Newfoundland Appalachians, *Program and Abstracts, 26th Annual Meeting, Northeastern Section*, Geological Society of America, Baltimore.

Ord, A. & Hobbs, B.E., 1989. The strength of the continental crust, detachment zones and the development of plastic instabilities, in *Deformation of Crustal Rocks*, pp. 269–289, ed. Ord, A., *Tectonophysics*, **158,** 269–289.

Pfiffner, O.A., Frei, W., Valasek, P., Stauble, M., Levato, L., DuBois, L., Schmid, S.M. & Smithson, S.B., 1990. Crustal shortening in the Alpine orogen: results from deep seismic reflection profiling in the eastern Swiss Alps, Line NFP 20-East, *Tectonics*, **9,** 1327–1355.

Phinney, R.A., 1986. A seismic cross section of the New England Appalachians: the orogen exposed, in *Reflection Seismology: the Continental Crust, Geodynamics Series*, Vol. 14, pp.

157–172, eds Barazangi, M. & Brown, L., Am. geophys. Un., Washington, DC.

Quinlan, G., Beaumont, C. & Hall, J., 1993. Tectonic model for crustal seismic reflectivity patterns in compressional orogens, *Geology*, **21**, 663–666.

Quinlan, G.M., Hall, J., Williams, H., Wright, J.A., Colman-Sadd, S.P., O'Brien, S.J., Stockmal, G.S. & Marillier, F., 1992. LITHOPROBE onshore seismic reflection transects across the Newfoundland Appalachians, *Can. J. Earth Sci.*, **29**, 1865–1877.

Rivers, T., Martignole, J., Gower, C.F. & Davidson, A., 1989. New tectonic divisions of the Granville Province, southeast Canadian Shield, *Tectonics*, **8**, 63–84.

Roure, F., Choukroune, P., Berastegui, X., Muñoz, J.A., Villien, A., Matheron, P., Bareyt, M., Seguret, M., Camara, P. & Deramond, J. 1989. ECORS deep seismic data and balanced cross sections: geometric constraints on the evolution of the Pyrenees, *Tectonics*, **8**, 41–50.

Rushmore, M.E. & Woodsworth, G.J., 1991. Coast Plutonic Complex: a mid-Cretaceous contractional orogen, *Geology*, **19**, 941–944.

Shelton, G. & Tullis, J., 1981. Experimental flow laws for crustal rocks, *EOS, Trans. Am. geophys. Un.*, **62**, 396.

Smith, E.G.C., Stern, T. & Reyners, M., 1989. Subduction and back-arc activity at the Hikurangi convergent margin, New Zealand, *Pageoph*, **129**, 203–231.

Stern, T.A. & Davey, F. J., 1989. Crustal structure and origin for basins formed behind the Hikurangi subduction zone of New Zealand, in *Origin and Evolution of Sedimentary Basins and their Energy and Mineral Resources, Geophys. Monogr. Ser.* 48, pp. 73–86, ed. Price, R. A., Am. geophys. Un., Washington, DC.

Stern, T.A., Quinlan, G.M. & Holt, W.E., 1992. Basin formation behind an active subduction zone: three-dimensional flexural modelling of Wanganui Basin, New Zealand, *Basin Res.*, **4**, 197–214.

Stockmal, G.S. & Waldron, J.W.F., 1990. Structure of the Appalachian deformation front in western Newfoundland: implications of multichannel seismic reflection data, *Geology*, **18**, 765–768.

Stockmal, G.S. & Waldron, J.W.F., 1991. Interpretations of Western Newfoundland Lithoprobe East lines: problems and possibilities for Humber Zone tectonics, in *Lithoprobe East Transect Report, Lithoprobe Report 23*, pp. 63–68, ed. Quinlan, G.M., LITHOPROBE Secretariat, University of British Columbia, Vancouver.

Varsek, J.L., Cook, F.A., Clowes, R.M., Journeay, J.M., Monger, J.W. H., Parrish, R.R., Kanasewich, E.R. & Spencer, C.S., 1993. Lithoprobe crustal reflection structure of the Southern Canadian Cordillera II: Coast Mountains transect, *Tectonics*, **12**, 334–360.

Wenzel, F., Sandemeier, K-J. & Walde, W., 1987. Properties of the lower crust from modelling refraction and reflection data, *J. geophys. Res.*, **92**, 11 575–11 583.

Willett, S., Beaumont, C. & Fullsack, P., 1993. A mechanical model for the tectonics of doubly-vergent compressional orogens, *Geology*, **21**, 371–374.